Am J Cancer Res 2023;13(1):143-160
www.ajcr.us /ISSN:2156-6976/ajcr0147089

Original Article

Using PDX animal models to identify and stratify adenoid cystic carcinoma patients presenting an enhanced response to HDAC inhibitors

Leticia DA Guimarães[1,2], Liana P Webber[1], Eduardo J Gaio[1,3], Decio SP Junior[2], Priscila Gonçalves[4], Michael J Wick[5], Nicole S Burr[6], Cristiane H Squarize[1,7], Rogerio M Castilho[1,7]

[1]Laboratory of Epithelial Biology, University of Michigan School of Dentistry, Ann Arbor, MI, USA; [2]Department of Stomatology, University of São Paulo, São Paulo, SP, Brazil; [3]Department of Periodontology, Federal University of Rio Grande do Sul, Porto Alegre, RS, Brazil; [4]Zucker School of Medicine at Hofstra/Northwell, Monter Cancer Center, Lake Success, NY, USA; [5]South Texas Accelerated Research Therapeutics, San Antonio, TX, USA; [6]Adenoid Cystic Carcinoma Research Foundation, Needham, MA, USA; [7]University of Michigan Rogel Cancer Center, University of Michigan, Ann Arbor, MI, USA

Received October 18, 2022; Accepted December 13, 2022; Epub January 15, 2023; Published January 30, 2023

Abstract: Adenoid cystic carcinoma (ACC) patients face a highly infiltrative and metastatic disease characterized by poor survival rates and suboptimal response to available therapies. We have previously shown that sensitization of ACC tumors to chemotherapy using histone deacetylase inhibitors (HDACi) constitutes a promising therapeutic strategy to manage tumor growth. Here, we used patient-derived xenografts (PDX) from ACC tumors to evaluate the effects of in vivo administration of the HDAC inhibitor Entinostat combined with Cisplatin over tumor growth. RNA from PDX tumor samples receiving the proposed therapy were analyzed using NanoString technology to identify molecular signatures capable of predicting ACC response to the therapy. We also used an RNAseq dataset from 68 ACC patients to validate the molecular signature identified by the NanoString platform. We found that the administration of Entinostat combined with Cisplatin resulted in a potent tumor growth inhibition (TGI) ranging from 38% to 106% of the original tumor mass. Enhanced response to therapy is consistent with the reactivation of tumor suppressor genes, including SFRP1, and the downregulation of oncogenes like FGF8 and CCR7. Nanostring data from PDX tumors identified a genetic signature capable of predicting tumor response to therapy. We further stratified 68 ACC patients containing RNAseq data accordingly to the activity levels of the identified genetic signature. We found that 23% of all patients exhibit a genetic signature consistent with a high ACC tumor response rate to Entinostat and Cisplatin. Our study provides compelling preclinical data supporting the deployment of a powerful systemic anticancer therapy crafted and explicitly tested for ACC tumors.

Keywords: Precision medicine, tumor genome landscape, histone, senescence, acetylation

Introduction

Adenoid cystic carcinoma (ACC) from the salivary glands is a rare malignancy characterized by a slow-growing, highly invasive, and metastatic potential. The high infiltrative and metastatic potential of the ACC from the salivary gland results in a long-term poor survival rate [1, 2]. The rarity of the ACC imposes a barrier to research efforts, halting our understanding of the biology of this disease. As a result, there is no consensus on the standard therapies used to manage ACC. Patients diagnosed with ACC may undergo extensive surgical resection, radiotherapy, chemotherapy, or a combination of these therapies. Radiotherapy has little effect on ACC, resulting in poor overall survival rates compared with surgery alone. Several drugs, including Cisplatin, have been used as a single chemotherapeutic agent, but the overall response rate is still low [3].

Emerging studies have shed light on the genetic landscape of ACC, showing a modest number of genetic alterations in primary tumors, while metastatic lesions present a complex genetic

landscape [1, 4-9]. ACC tumors often present gene fusion of *MYB-NFIB* and *MYBL1-NFIB* and mutations in the *NOTCH1* gene. Interestingly, the genetic landscape of ACC also shows important mutations of genes involved in the epigenetic control of cellular functions [10]. Among several epigenetic mechanisms, histone acetyltransferase (HAT) and histone deacetylase (HDAC) play a critical role in chromatin remodeling. Dysregulation of HDAC is found in many malignancies, including neuroblastomas, medulloblastomas, lung adenocarcinomas, and breast and prostate cancers, among others [11]. We have previously shown that the HDAC inhibitor Vorinostat combined with Cisplatin halted the viability of ACC primary tumor cells *in vitro* [12].

Here, we decided to investigate the use of low doses of Entinostat, a selective HDAC inhibitor targeting class I HDAC, as an ACC sensitizer agent to Cisplatin in the PDX animal model. We found that the combination of Entinostat and Cisplatin resulted in a potent tumor growth inhibitory effect (TGI) of ACC tumors ranging from 38% to 106% compared with controls. Furthermore, we identified the molecular changes involved in the tumor response to the combination therapy using a Pan-Cancer Pathways Panel from the NanoString platform. We found that ACC tumors presenting a greater response to Entinostat and Cisplatin therapy exhibited a unique activity level of the Cell Cycle/Apoptosis and the PI3K signaling pathways. We further decided to validate our findings by stratifying a cohort of 68 ACC tumor patients containing RNAseq data using our newly established genetic signature.

Altogether, our data indicated that the combination of Entinostat and Cisplatin constitutes a promising therapeutic strategy for managing patients with ACC. We also identified the cell cycle/apoptosis and PI3K pathways as a genetic signature capable of stratifying ACC patients, presenting an enhanced response to the proposed therapy.

Material and methods

Patient-derived xenograft (PDX) and drug dilution

Patient-derived xenograft (PDX) models were housed at the South Texas Accelerated Research Therapeutics (START, San Antonio, TX) and performed under protocols approved by the START IACUC. Briefly, human tumor fragments from 3 patients (ACCX9; ACCX5M1; ACCX6) were transplanted subcutaneously into the dorsal region of male severe combined immunodeficient (SCID) mice as previously reported [13]. ACCX9 advent from a grade 3 primary tumor of the parotid gland; ACCX5M1 and ACCX6 are metastatic grade 2 tumors isolated from the lungs and primarily originated from the oral cavity and the parotid gland, respectively. ACCX9 and ACCX5M1 present *NFIB* translocation to the *MYB* locus, while ACCX6 does not present *NFIB* translocation. Mice receiving the human tumor fragments from ACCX5M1, ACCX6, and ACCX9 were randomized into 4 groups per tumor. They received either vehicle, Entinostat (5 mg/kg), Cisplatin (3 mg/kg), or the combination of Entinostat (5 mg/kg) and Cisplatin (3 mg/kg) for 3 weeks (**Figure 1A**). For the combined administration of Entinostat and Cisplatin, tumors were sensitized with Entinostat 6 days prior to the administration of Cisplatin. PDX mice received daily oral administration of vehicle or Entinostat and a weekly administration of intraperitoneal Cisplatin for 2 weeks. Entinostat was diluted in 0.5% methylcellulose solution in saline under sonication. Cisplatin was diluted in 0.5% HCL solution. Tumor growth was monitored and measured every 3 days. Tumor growth inhibition (TGI) was calculated by comparing the tumor volume of each therapeutic arm with the vehicle group.

RNA extraction, NanoString nCounter assay, and data analysis

Tumor samples from all ACC PDX mice and conditions were embedded in OCT and stored at -80°C. Frozen samples from the PDX tumors and therapeutic conditions were sectioned in 7 µm thickness and processed for RNA extraction using the Quick-RNA MicroPrep Kit (Zymo Research, USA). The total amount of RNA was quantified using a Qubit fluorometer (Nanodrop, USA) and Nanodrop (Thermo Scientific, USA). RNA from all samples was diluted to a final concentration of 100 ng/5 µL. RNA samples were multiplexed using a nCounter Pan-Cancer Pathway Panel (NanoString, USA) containing 770 genes distributed in 13 cancer-related signaling pathways (i.e., MAPK, STAT,

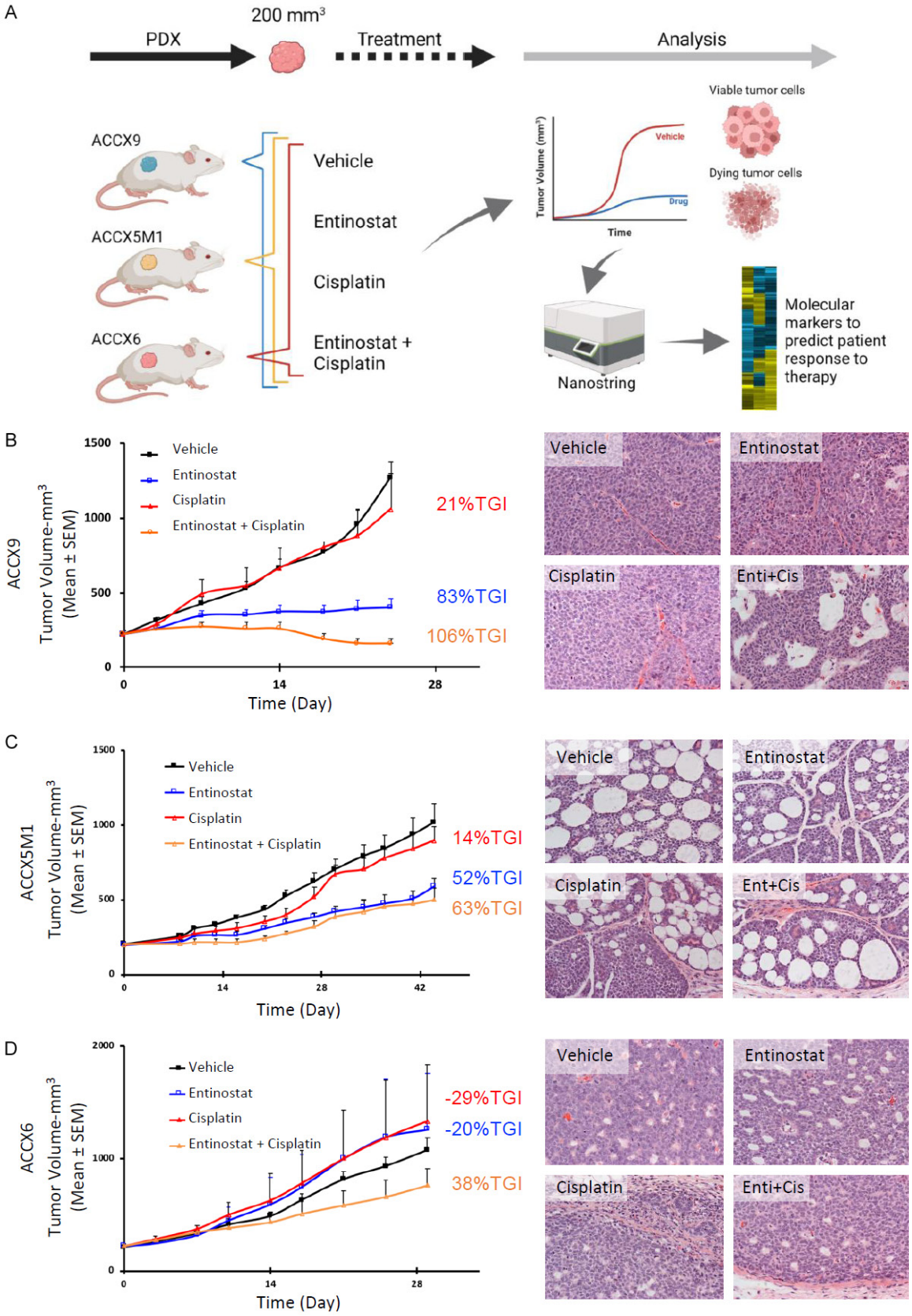

Figure 1. Therapeutic efficacy of Entinostat/Cisplatin in ACC PDX models. (A) Graphical representation of study design. Briefly, patient-derived ACC tumors (ACCX6, ACCX5M1, ACCX9) were transplanted subcutaneously into the

dorsal region of severe combined immunodeficient mice (SCID mice). After reaching 200 mm^3, each ACC patient-derived xenograft (PDX) was treated with vehicle (control) and the 3 therapeutic arms (i.e., Cisplatin alone, Entinostat alone, or Entinostat/Cisplatin combination therapy). Tumor growth was monitored and measured every 3 days. Tumor growth inhibition (TGI) was calculated by comparing the tumor volume of each therapeutic arm with the vehicle group. Tumor samples were processed for histology and assessment of gene and protein expressions. (B-D) Graphs depict the volume of PDX tumors generated with human ACCX6 (B), ACCX5M1 (C), and ACCX9 (D) treated with each of the 3 therapeutic arms and vehicle (control). TGI is shown next to the therapeutic arm line. Note that the combination therapy displayed the most effective TGI. Data represent mean values (± SEM) of 8 PDX and experimental conditions. Morphological changes of ACC tumors upon each therapeutic arm are depicted H&E. Note changes in the tumor morphology upon administration of Entinostat/Cisplatin for ACCX9.

PI3K, RAS, TGF-β, cell cycle, apoptosis, Hedgehog, Wnt, DNA damage control, transcriptional regulation, and chromatin modification). Data output (raw data) was analyzed using nSOLVER Analysis Software containing the Advanced Analysis 2.0 plugin (NanoString, USA). Quality control of raw data was performed by combining Imaging QC, reporter probe density (Binding Density QC), measurement of internal positive control, and limit of detection. Normalization was carried out automatically by using the geometrical mean of positive controls and the normalization genes from the CodeSet content. Fold change, or ratio, was calculated using vehicle-treated tumors and compared with all treatment groups. Volcano plot, direct global significance pathway analysis, and pathway scores were calculated using the Advanced Analysis 2.0 plugin (NanoString, USA) in a Windows operating system and R environment (The R Foundation). Direct global significance pathway analysis and pathway scores were calculated using the Advanced Analysis 2.0 plugin (NanoString, USA) in a Windows operating system and R environment (The R Foundation). Normalized data from nSOLVER (Log2) was imported into Cluster 3.0 and centered for genes (Center Genes). Hierarchical clustering (uncentered) was performed for Genes and Arrays followed by average linkage. Data output from Cluster 3.0 was uploaded into Java TreeView software to visualize and extract gene lists following clustering patterns.

Immunohistochemistry and immunofluorescence staining

Histological sections cut at 4 μm thickness from each PDX sample and treatment condition were processed for immunohistochemistry. Briefly, histological sections were deparaffinized in xylene substitute solution and hydrated in descending grades of ethanol, followed by incubation with 3% (w/v) bovine serum albumin (BSA) and 0.5% (v/v) Triton X-100 in PBS. Primary antibody anti-p16 (1:50, BD Biosciences #550834, San Jose, CA, USA) was incubated overnight, followed by the secondary anti-mouse antibody (Vector Laboratories, Burlingame, CA, USA) at room temperature (RT) 60 min. DAB detection system (3,3'-Diaminobenzidine) was used, followed by hematoxylin Counterstain. Immunofluorescence staining was carried out after histological sections were deparaffinized, hydrated, and incubated in 3% BSA and 0.5% Triton X100 in PBS. Tissue samples were incubated overnight using the primary antibodies anti-Ki67 (AFFN-Ki67-3EG, DSHB, Iowa, USA), γ-H2AX (EMD Millipore, Burlington, USA), Acetyl-Histone H4 (Lys5), Acetyl-Histone H4 (Lys8) (Thermo Scientific, Waltham, MA), Acetyl-Histone H4 (Lys12), Acetyl-Histone H3 (Lys9) Acetyl-Histone H4 (Lys16), and Caspase 3 (Cell Signaling Technology, Danvers, MA, USA). Next, slides were incubated for 60 min at RT with Alexa 488 or Alexa 568 anti-rabbit and counterstained with Hoechst 33342 (Invitrogen, Carlsbad, CA, USA). Images were taken using a QImaging ExiAqua monochrome digital camera attached to a Nikon Eclipse 80i microscope (Nikon, Melville, NY) and visualized on the Nikon NIS Elements software and captured at 200× final magnification.

Cohort of 68 ACC patients, Nanostring-RNAseq analysis

RNAseq data set was graciously provided by Dr. Scott A. Ness from the University of New Mexico. Briefly, the dataset was constituted of 68 samples from 30 female and 38 male patients with a mean age of 50.1 years at surgery [14]. The University of Michigan Bioinformatics Core performed two distinct analyses using the RNAseq data. The analysis compared the genes expression of the RNAseq dataset from 68 patients with the Nanostring gene set that composes the two most discrimi-

native pathways for the PDX Nanostring data ('Cell Cycle + Apoptosis' and 'PI3K') and determined patient sample stratifications based on the pathway summaries. Briefly, all analysis and graphics were generated in R (v 3.6.1). Count table containing a total of 68 samples was annotated with meta-data downloaded from the NCBI's SRA Run Selector for NCBI BioProject ID: PRJNA287156. The count table was then filtered to retain only genes with at least 250 counts across all samples and normalized using the DESeq2 package (v 1.26.0) and by specifically applying the "vst" function for FFPE data analysis [15, 16]. The normalized and raw count tables were further processed to subset to genes annotated by Nanostring to be part of one or more of three specific pathways of interest: Cell Cycle-Apoptosis, and PI3K. Pathway gene member expression in each sample, statistics for the vst normalized gene counts were generated for each sample with the pastecs package using the 'stat.desc' function (v 1.3.21). The vst normalized count table described above was further processed to subset to genes annotated by Nanostring to be part of one or more of three specific pathways of interest: 'Cell Cycle-Apoptosis' and 'PI3K'. Individual samples were labeled either based on top/bottom expression in the pathway or after stratification above/below the mean expressions of each pathway, where ACCX9-like samples were classified as samples that had both average expression for the Cell Cycle pathway above the mean and average expression for the PI3K pathway below the mean with samples classified as ACCX5M1-like had the opposite expression pattern.

Veen graphics, oncogene database, TSGene database, RNA seq data, and statistical analysis

Veen graphics were created using the online tool Venny 2.0 (Oliveros, J.C., 2007-2015, Venny. An interactive tool for comparing lists with Venn's diagrams. Publicly available at http://bioinfogp.cnb.csic.es/tools/venny/index.html). The list of 803 known oncogenes and 1217 human tumor suppressor genes were from the Oncogenm (http://ongene.bioinfo-minzhao.org/index.html) [17] and TSGene databases https://bioinfo.uth.edu/TSGene/download.cgi?csrt=7154395379350750750 [18], respectively.

Statistical analysis was performed using GraphPad Prism (GraphPad Software, San Diego, CA, version 8). Immunofluorescence quantification of the total number of positive cells was performed using one-way ANOVA followed by Tukey's multiple comparison tests. Asterisks denote statistical significance (*P≤0.05; **P≤0.01; ***P≤0.001; ****P≤0.0001) and ns (P≥0.05). Heatmap of Directed Global Significance Score (**Figure 3D**) displaying each sample's global significance scores and directed global significance scores. The global significance score was calculated as the square root of the mean squared t-statistic for the genes in a gene set, with t-statistics coming from the linear regression underlying our differential expression analysis.

Results

Sensitization therapy using the HDAC inhibitor Entinostat prior to Cisplatin results in tumor growth inhibition in PDX tumor models

Patient-derived xenograft (PDX) models constitute the best preclinical models for emerging therapies as they best recapitulate the human tumor response to therapy [19]. PDX models contain both human tumor cells and their microenvironment. ACC PDX models (ACCX6, ACCX9, and ACCX5M1) received the single agents' Entinostat, Cisplatin, or vehicle, as well as the Entinostat and Cisplatin combination therapy (**Figure 1A**). We also started administration of Entinostat 6 days prior to the administration of Cisplatin to elicit sensitization of tumors. The ACC PDX models had an improved response to the combined therapy with enhanced TGI than any single-agent therapies (Entinostat or Cisplatin alone) (**Figure 1B-D**). ACCX9 tumor response to combined therapy was excellent, with an overall TGI of 106% over the original implanted tumor size (150-300 mm^3). Histologically, ACCX9 presented a solid growth pattern that is found altered upon the administration of the combined therapy of Entinostat and Cisplatin (**Figure 1B**_H&E). ACCX5M1 and ACCX6 tumors responded to the combination therapy with an overall TGI of 63% (**Figure 1C**_H&E) and 38% (**Figure 1D**_H&E), respectively. Upon therapy, there was no change in the histological pattern of either ACCX5M1 or ACCX6. Administration of Entinostat as a single agent was the second most

successful therapy for ACCX9 and ACCX5M1, with an 83% and a 52% TGI, respectively. However, Entinostat alone failed to induce any TGI in ACCX6 tumors. Administration of Cisplatin alone was the least effective therapy for ACC. While ACCX9 tumors showed a 21% TGI with Cisplatin, ACCX5M1 presented a 14% TGI, and ACCX6 tumors completely failed to respond to Cisplatin (**Figure 1B-D**).

From a biological perspective, the sensitization of ACC tumors with Entinostat followed by the administration of Cisplatin resulted in an overall reduction of ACCX9 and ACCX5M1 proliferative potential (**Figures 2A**, S1A, *P<0.05, ****P<0.0001). ACCX6 tumor did not present a reduction in its proliferative potential compared to the control (ns P>0.05). Tumor apoptosis was assessed using the caspase 3 marker (**Figures 2B**, S1B). Interestingly, ACCX9 tumors had an overall higher count of apoptotic cells in all therapeutic arms than ACCX5M1 and ACCX6 (****P<0.0001). Interestingly, the administration of Entinostat as a single agent was the best therapeutic modality to induce apoptosis in all ACC tumors (**P<0.01, ****P<0.0001).

DNA double-strand breaks (DSB) are responsible for triggering the DNA repair machinery while preventing the accumulation of misrepaired DSB. However, actively repairing DNA in cancer cells can allow cancer to survive chemotherapy [20, 21]. Here, we assessed the effect of the therapies on DSB repair machinery using γ-H2AX. The accumulation of γ-H2AX is a strong indication of active DNA DSB. We observed that either the HDAC inhibitor Entinostat administered alone or in combination with Cisplatin could reduce the DSB load on ACCX9 (**P<0.01) and ACCX5M1 (*P< 0.05; **P<0.01) (**Figures 2C**, S1C) tumors. ACCX6 tumors showed a similar trend with the combined administration of Entinostat in combination with Cisplatin, although not statistically significant (**Figures 2C**, S1C, ns P>0.05).

Identification of molecular markers associated with tumor response to Entinostat and Cisplatin combination therapy

In order to identify clinically relevant genes with biomarker potential for clinical stratification of patients, we performed gene clustering analysis and identified 2 clusters of interest: Cluster 1 is characterized by the downregulation of genes in all 3 PDX models, while cluster 2 presents genes upregulated (**Figure 3A**). From the 130 genes found downregulated and 127 genes found upregulated in all PDX models (ACCX9, ACCX6, and ACCX5M1) upon administration of Entinostat and Cisplatin, we focused on the identification of known oncogenes and tumor suppressor genes as potential biomarkers. Specifically, we are interested in oncogenes that have their expression directly impacted by our combined therapy and tumor suppressor genes that became activated upon therapy. Our initial analysis focused on cluster 1, comparing 130 downregulated genes with a database of 803 known human oncogenes (ONgene Database) [17]. We identified 26 oncogenes presenting 2-fold downregulation upon administration of Entinostat in combination with Cisplatin (Figure S2). Among all oncogenes presenting 2-fold downregulation in each PDX model, we found that FGF8 was the only oncogene commonly downregulated in all 3 PDX models (**Figures 3B**, S2). FGF8 is a known oncogene that can transform NIH3T3 cells leading to tumor growth in vivo, and it cooperates with WNT1 signaling during mammary tumorigenesis [22, 23].

Looking into cluster 2, Entinostat combined with Cisplatin triggered the upregulation of several tumor suppressor genes in each PDX model (n = 127) (**Figure 3A**). Genes identified in cluster 2 were matched against a Tumor Suppressor Gene (TSG) database (TSGene Database) [18]. We identified 31 TSG presenting upregulated upon administration of Entinostat and Cisplatin (Figure S3). Nine of the TSG were upregulated over 2-folds on ACC tumors, including CDH1/E-Cadherin, CDKN1C, CEBPA, MAPK9/JNK2, NFKB1, NUPR1, PRKAA2/AMPK, and SFRP1. SFRP1 was found upregulated in all PDX models (**Figures 3C**, S3). Secreted frizzled-related protein 1 (SFRP1) regulates the WNT pathway by competing with Frizzled receptors for WNT binding [24, 25]. SFRP1 is deregulated in several tumors, including invasive breast carcinomas, hepatocellular carcinoma, clear cell renal cell carcinoma, and non-small-cell lung cancer [26-29].

Although all ACC tumors responded well to the combination therapy, it is evident that the ACCX9 tumor responded significantly better,

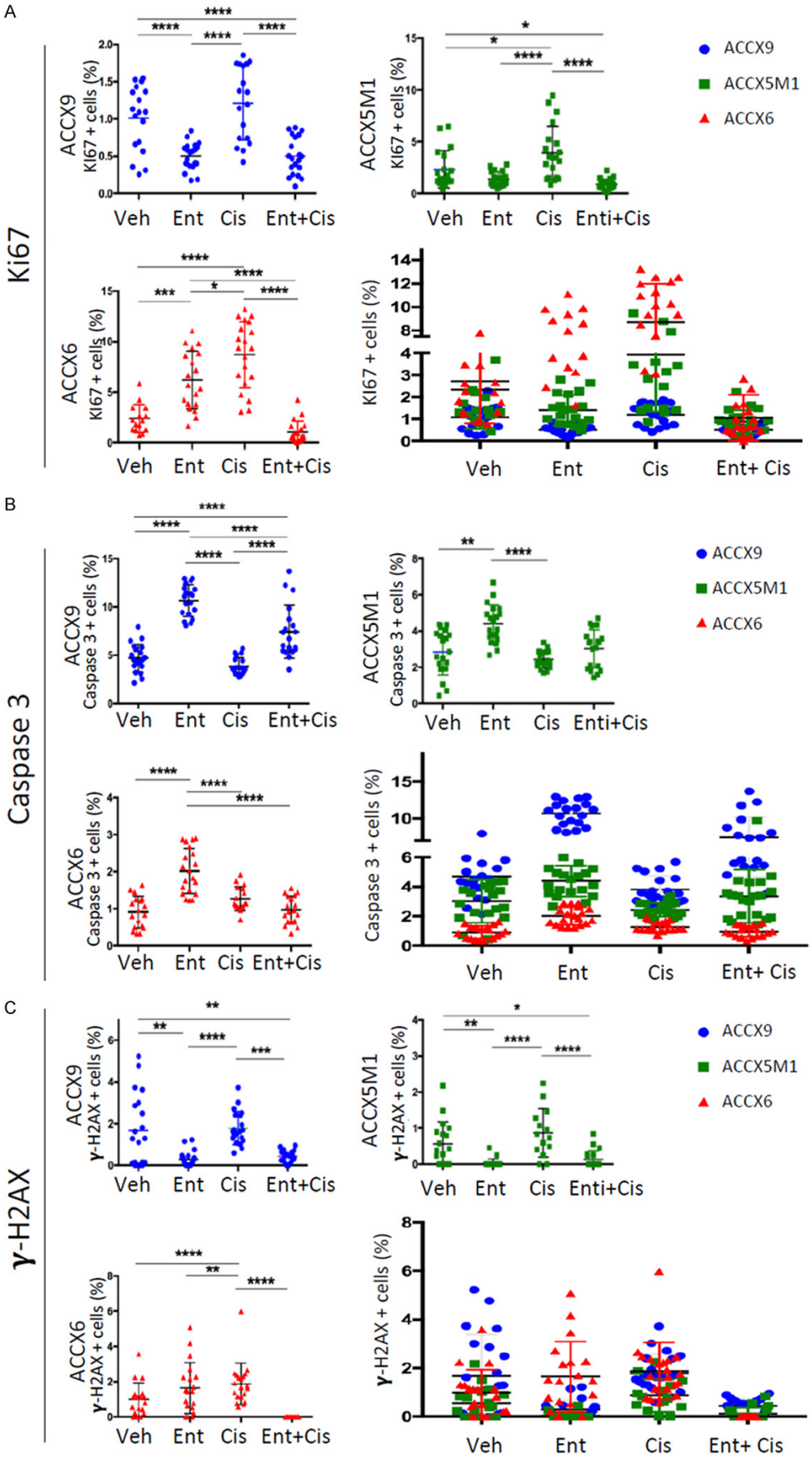
A
Ki67
ACCX9
KI67 + cells (%)
Veh
Ent
Cis
Ent+Cis
ACCX5M1
Enti+Cis
ACCX6
Ent+ Cis
ACCX9
ACCX5M1
ACCX6
B
Caspase 3
Caspase 3 + cells (%)
C
γ-H2AX
γ-H2AX + cells (%)

Figure 2. The effect of the therapeutic arms on tumor proliferation, apoptosis, and DNA repair. (A) Cellular proliferation was assessed using Ki67 staining, (B) while the levels of cellular apoptosis from all PDX models were assessed using Caspase 3, and (C) content of DNA damage was assessed using γ-H2AX markers. Quantification of each marker is depicted as positive cells per field for each tumor, or as a combination of all tumors (*P<0.05; **P<0.01; ***P<0.001; ****P<0.0001).

presenting a TGI of 106% (**Figure 1B**) and a distinct genetic signature. With that, we focused on identifying genes differentially regulated in ACCX9 compared to ACCX5M1 and ACCX6 tumors (**Figure 3D**). Cluster 3 are genes found upregulated in ACCX9 and downregulated in ACCX5M1 and ACCX6 (**Figures 3E**_TSG; S4A_ cluster 3). The activation (2-fold expression) of the tumor suppressor genes PPARG, WT1, MAP3K8, and WNT5A were present within cluster 3 (**Figure 3E**). In cluster 4, we identified genes downregulated in ACCX9 and upregulated in ACCX5M1 and ACCX6 (**Figures 3F**; S4B_ cluster 4). These identified genes were oncogenes presenting over 2-fold downregulation, like PDGFRA, TGFB1, PDGFB, and FZD2.

Identifying the efficacy of Entinostat and Cisplatin on inducing histone acetylation on adenoid cystic carcinomas

The effect of Entinostat on ACC tumors and gene transcription can be accessed by its ability to acetylate histones. Histones H3 and H4 are part of the core histones presenting multiple acetylation sites, and the post-translation modification of histone acetylation is well-known to induce transcription activation [30, 31]. It is important to note that the baseline acetylation levels of all PDX tumors vary greatly (**Figures 4A-E**, S5 and S6_Vehicle). Here we asked if the differences in the tumor responses to Entinostat/Cisplatin correlate with the degree of histone acetylation found in ACC samples after treatment. Overall ACCX9 tumors (TGI: 106%) showed greater acetylation levels of histones than ACCX6 (TGI: 38%), while ACCX5M1 (TGI: 63%) stayed in the middle of the pack. Considering the baseline expression levels of each PDX model, ACCX9 tumors were acetylated upon administration of Entinostat/Cisplatin for histones H3K9, H4K5, and H4K8. ACCX5M1, on the other hand, presented enhanced histone acetylation for H3K9, H4K12, and H4K16. Interestingly, however, ACCX6 PDX presenting the lowest TGI failed to respond to any therapy resulting in low histone acetylation levels compared with vehicle levels (**Figures 4A-E**, S5 and S6).

In a side-by-side comparison, it became clear that histones from ACCX6 tumors are completely unresponsive to the histone deacetylase inhibitors Entinostat (**Figures 4F-J**, S7).

Senescent tumor cells accumulate in PDX models presenting reduced TGI response

We have previously shown that in vitro administration of HDAC to ACC primary cells results in the activation of cellular senescence [12]. Here we sought to understand if the accumulation of senescent cells observed in ACC tumors is associated with tumor resistance to therapy. Using the cellular senescence marker $p16^{ink4}$, we observed that administration of Entinostat/Cisplatin resulted in the accumulation of senescent cells exclusively in ACCX6 tumors (**Figure 5A**, **5B**, ****P<0.0001). ACCX9 and ACCX5M1 responded to therapy by reducing the number of cells undergoing senescence (**Figure 5A**, **5B**, ***P<0.001, ****P<0.0001).

Identification of signaling pathways capable of predicting enhanced tumor response to the proposed therapy

After we learned that the three therapeutic arms (i.e., Cisplatin, Entinostat, and the combination of both drugs) differentially impact tumor growth (**Figure 1B-D**) and that the ACCX9 PDX model responds remarkably well to the combined therapy, we sought to identify biomarkers capable of stratifying patients with favorable clinical outcome.

Using a pathway score function from nSOLVER Analysis Software, we observed 2 distinct patterns associated with the activity levels of all major signaling pathways (**Figure 6A**). One pattern was associated with ACCX9 PDX tumors presenting a better response to therapy (TGI: 106%), containing an enhanced global expression of genes associated with cell cycle/apoptosis and DNA damage repair pathways. The second pattern was associated with tumors presenting a reduced response to therapy (TGI: 63% and 38%) and enhanced activity levels associated with other 10 cancer-related pathways (i.e., Hedgehog, JAK-STAT, MAPK, Notch,

A

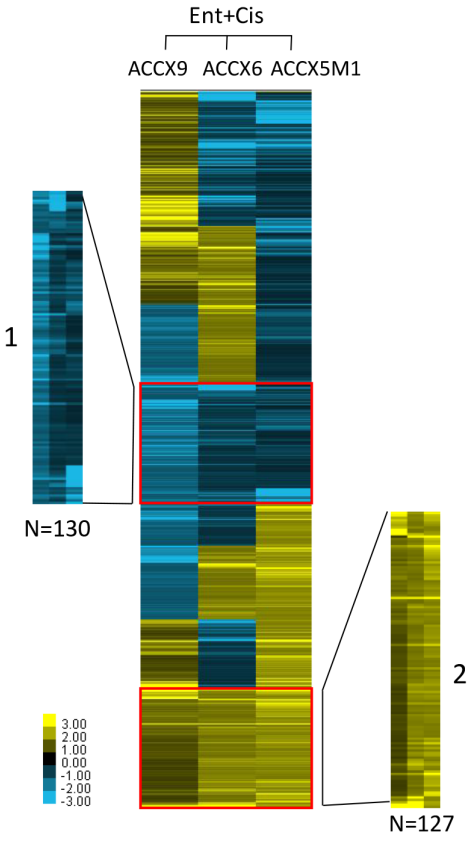

B

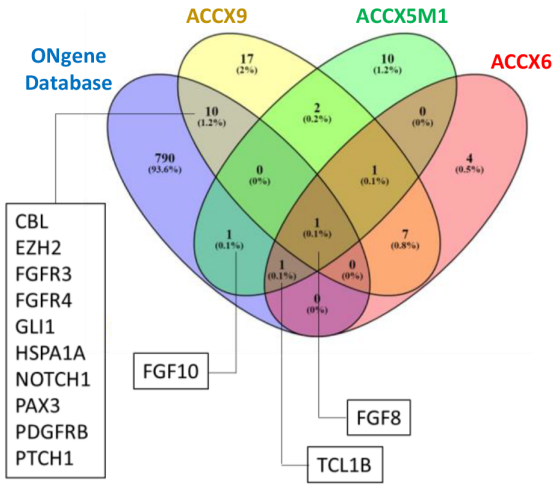

C

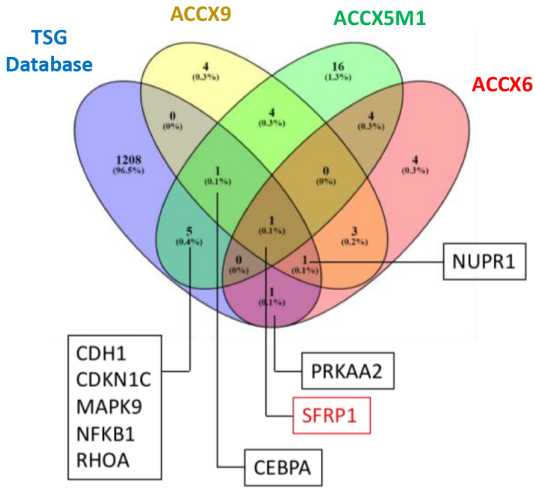

D

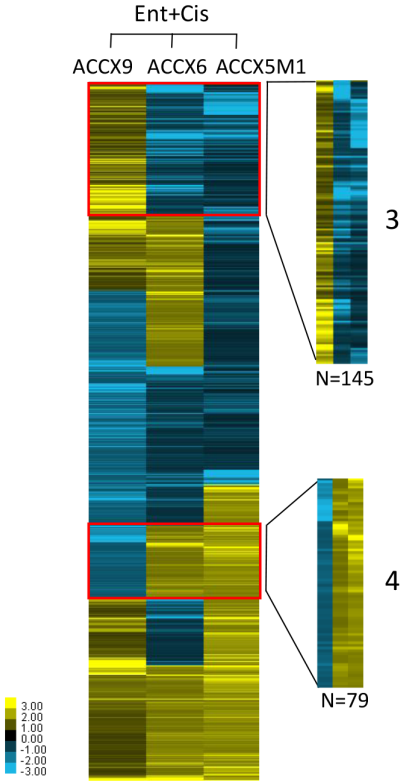

E

ACCX9 upregulated TSG (over 2-fold)

Probe Name	ACCX9	ACCX6	ACCX5M1
PPARG	2.861234	-1.36134	-0.91997
WT1	2.861234	-1.03134	-1.09997
MAP3K8	2.651234	-1.92134	-1.01997
WNT5A	2.551234	-0.94134	-0.86997

F

ACCX9 downregulated oncogenes (under 2-fold)

Probe Name	ACCX9	ACCX6	ACCX5M1
PDGFRA	-3.85877	1.758662	2.020026
TGFB1	-2.82877	1.338662	1.630026
PDGFB	-2.35877	1.838662	1.760026
FZD2	-2.07877	1.408662	1.720026

Figure 3. Tree view analysis of ACC tumors receiving combination therapy. A. Gene clustering of ACCX9, ACCX5M1, and ACCX6 receiving Entinostat combined with Cisplatin according to gene expression (baseline) from the vehicle group. The blue color denotes genes downregulated in all ACC tumors (cluster 1), and the yellow color denotes genes upregulated in all ACC tumors following. B. Genes found downregulated (2-fold) in cluster 1. Note that all depicted genes are classified as oncogenes. C. List of genes upregulated in all ACC tumors (cluster 2). Note that depicted genes denote tumor suppressor genes. D. Clusters 3 and 4 represent genes found upregulated (n = 145) and downregulated (n = 79), respectively, in the ACCX9 PDX model characterized by a tumor growth inhibition of 106% upon administration of Entinostat/Cisplatin. E. Table derived from cluster 3 depicts tumor suppressor genes (TSG) presenting 2-fold upregulation on ACCX9 compared with ACCX6 and ACCX5M1 tumors upon administration of Entinostat/Cisplatin. F. Table derived from cluster 4 depicts oncogenes presenting a 2-fold downregulation on ACCX9 compared with ACCX6 and ACCX5M1 tumors upon administration of Entinostat/Cisplatin.

PI3K, Ras, TGF-beta, Transcription Misregulation, Wnt, and Driver genes) (**Figure 6A**).

Interestingly the group of genes that comprises the chromatin modification pathway show enhanced global levels for ACCX9 and ACCX5M1, both models presenting TGI superior of 63% (**Figure 6A**_light blue line), and thereby excluding PDX tumors presenting lower TGI (ACCX6).

Furthermore, we have identified TNFRSF10C and PPP2R2C as two potential biomarkers (members of the cell cycle & apoptosis pathway) highly expressed in ACCX9 (TGI: 106%) and downregulated in ACCX5M1 (TGI: 63%) and ACCX6 (TGI: 38%) tumors (**Figure 6B**). Using a similar approach, we identified 15 relevant genes found downregulated in the ACCX9 tumor (2-fold decrease) and upregulated in ACCX5M1 and ACCX6 tumors. From all 15 genes, NGF, PDGFA, and FGF1 were found to be commonly expressed in the PI3K, RAS, and MAPK signaling pathways (**Figure 6C**).

Perhaps the most exciting findings from this study are not only the identification of unique biomarkers with potential clinical relevance but rather the understanding that activity levels of signaling pathways constitute a robust predictor of tumor response to therapy (**Figure 6A**). Indeed, the expression of each signaling pathway is not significantly influenced by different treatments. With that in mind, we decided to validate our findings using RNAseq data from 68 ACC patients. We decided to stratify all ACC patients using the collection of genes from the NanoString platform that constitutes the cell cycle/apoptosis and the PI3K pathways. We successfully stratified ACC patients presenting high activity levels of the cell cycle-apoptosis pathway and low activity of the PI3K signaling suggesting similar molecular signatures from ACCX9 PDX tumors (**Figure 6D**_blue dots). Similarly, we successfully stratified patients expressing high activity levels of the PI3K pathway and low cell cycle-apoptosis levels, similar to the ACCX5M1 PDX tumors (**Figure 6D**_red dots). Overall, we found that 23% of the 68 ACC patients containing RNA seqdata fit the genetic profile of PDX tumors, presenting an enhanced response to therapy (ACCX9 profile: TGI of 106%) (**Figure 6E**). Also, 15% of all patients fit the PDX genetic profile of ACCX5M1 presenting a TGI of 63% (**Figure 6E**). The remaining 62% of all ACC patients do not fit either genetic profile.

Discussion

Recent efforts in understanding the genetic landscape of ACC of the salivary gland unveiled the high incidence of *MYB-NFIB* translocations and the somatic mutations in *MYB*-associated genes [5, 8, 9]. Although several mutations have been identified, ACC tumors are mainly characterized by the low presence of mutations, particularly when compared with other solid tumors [9]. These findings suggest that the carcinogenesis process of ACC is likely associated with fewer driver oncogenes like MYB instead of high genomic instability [32, 33]. Along with the activation of MYB, there is strong evidence of the deregulation of the epigenetic machinery. Indeed, close to 35% of ACC tumors present mutations in chromatin remodeling genes [9]. Here we explored the potential effects of the HDAC inhibitor Entinostat on an ACC preclinical model. Similar to what we observed in ACC primary tumor cells in culture [12], induction of histone modifications before the administration of Cisplatin resulted in superior tumor growth inhibition compared with the administration of Entinostat or Cisplatin as single agents.

Using NanoString technology, we quantified the native RNA content of each tumor model and characterized the impact of the treatment arms

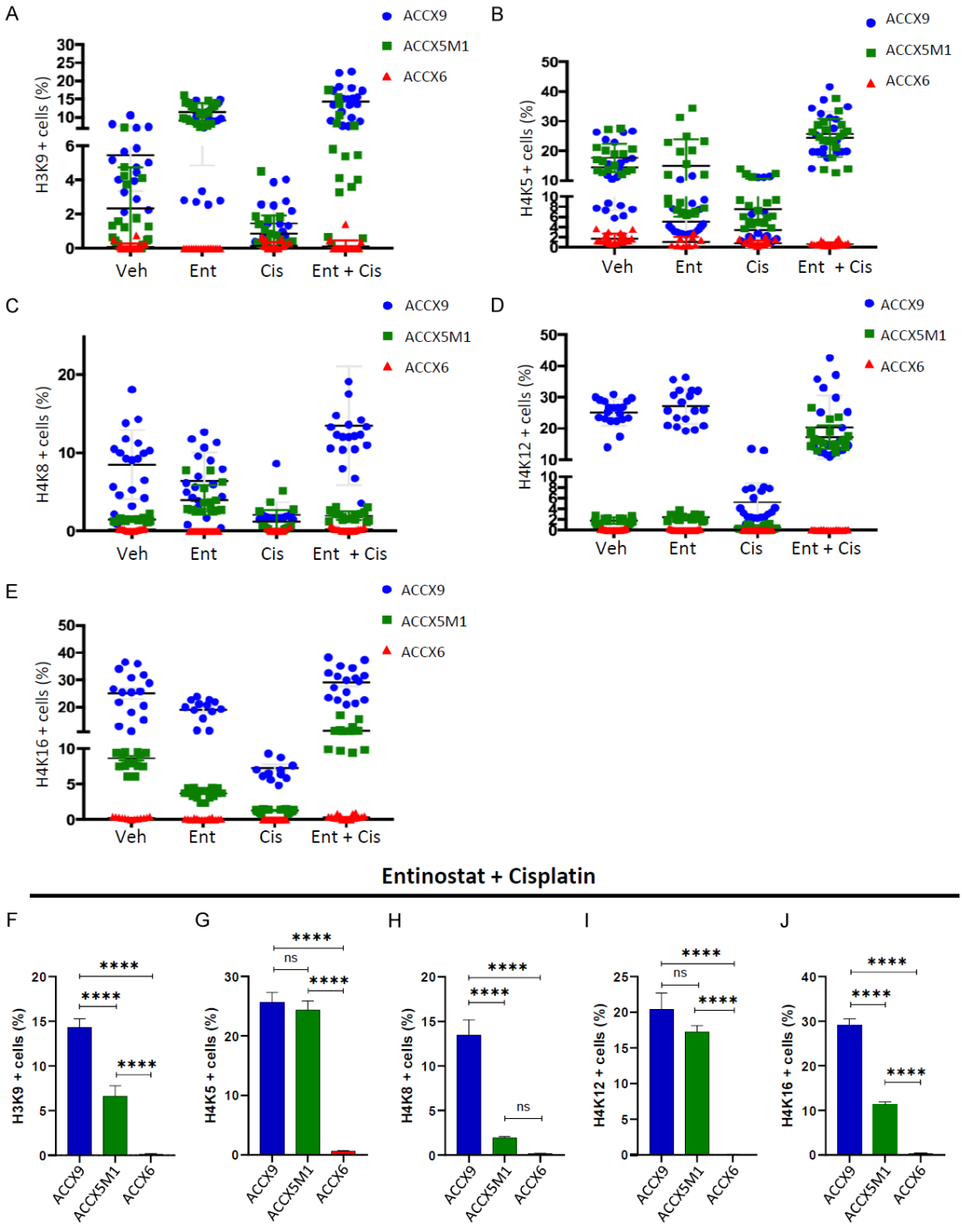

Figure 4. Pharmacological effect of combination therapy on global tumor histone acetylation. Quantification of immunofluorescence staining for histone H3 and H4 at multiple acetylation sites, including histone H3 Lysine 9 (A), histone H4 lysine 5 (B), histone H4 lysine 8 (C), histone H4 lysine 12 (D), histone H4 lysine 16 (E) in tumor samples receiving Entinostat, Cisplatin, and the combination therapy of Entinostat/Cisplatin. (F-J) Comparison between all 3 PDX tumor model responses to Entinostat/Cisplatin. Note the reduced effect of combination therapy over ACCX6 when compared with high acetylation levels observed in ACCX6 and, to some extent, ACCX5M1 (*P<0.05; **P<0.01; ***P<0.001; ****P<0.0001).

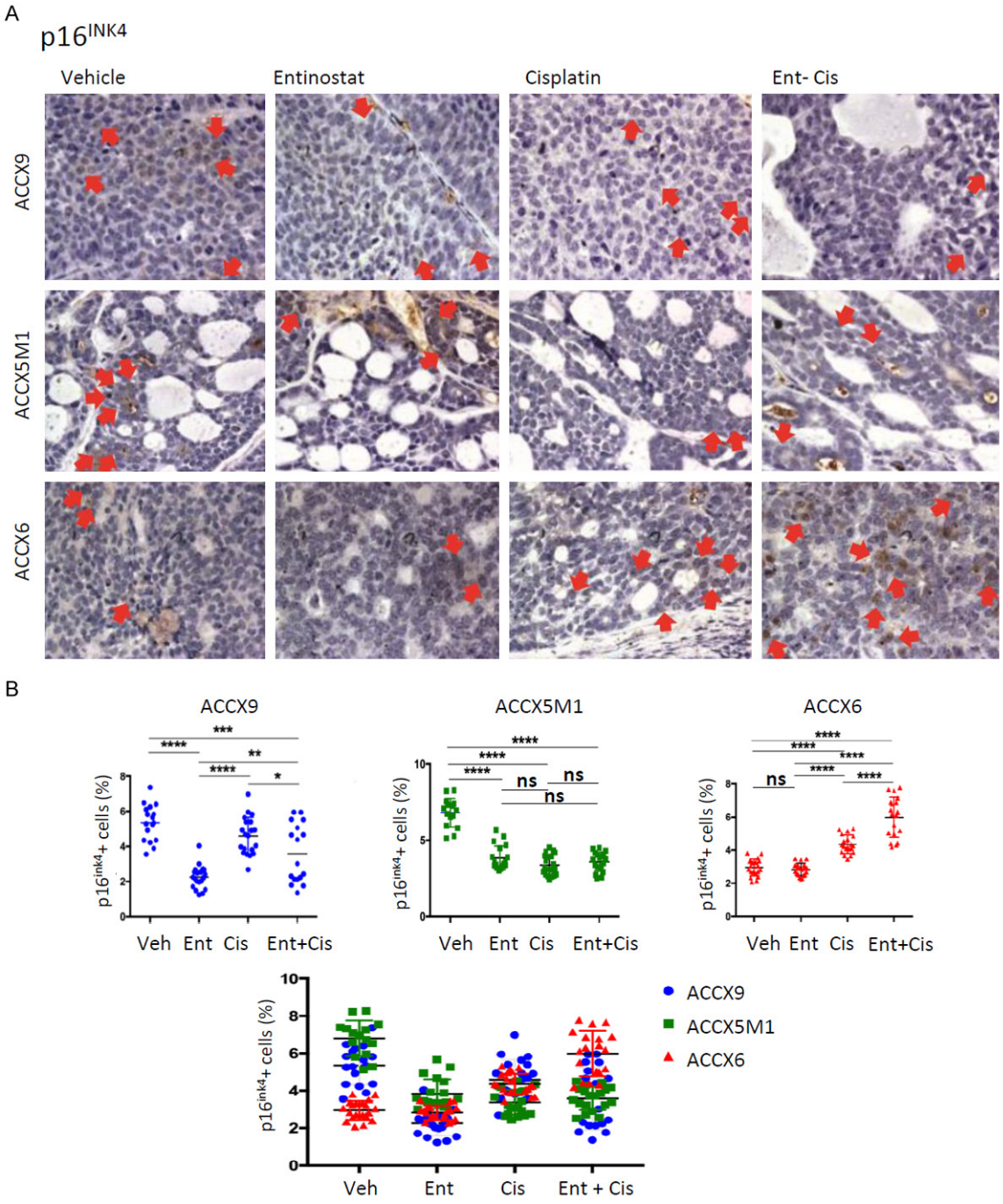

Figure 5. Activation of Cellular Senescence in ACC PDX tumors. A. Immunohistochemical staining of PDX tumors for cellular senescence using $p16^{ink4}$. Red arrows indicate positive cells for staining. B. Quantification of immunohistochemical staining of PDX tumors for the cellular senescence marker $p16^{ink4}$. Quantification depicts the percentage of positive cells per field of each PDX model or as a combination of all tumors upon administration of Cisplatin, Entinostat, Entinostat/Cisplatin, or vehicle as control (*P<0.05; **P<0.01; ***P<0.001; ****P<0.0001).

on the activation of key cancer-related molecular pathways. We observed that the combination therapy of Entinostat and Cisplatin was the most efficient treatment, and showed significant downregulation of several oncogenic signaling pathways compared with Cisplatin, currently the most used chemotherapy agent for ACC. When looking into the entire set of PDX

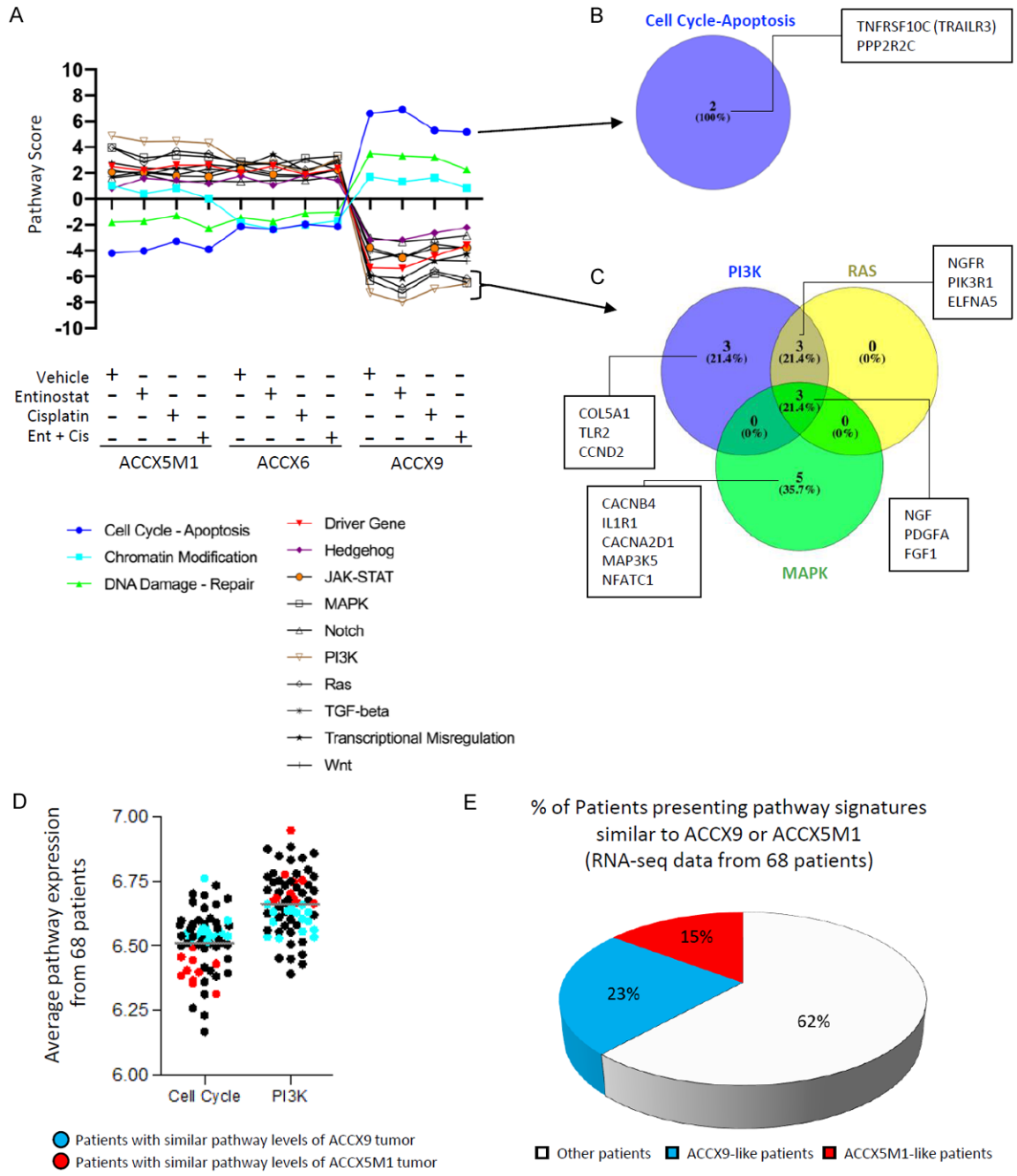

Figure 6. Identifying signaling pathways as genetic signatures for treatment success and validation of findings using a cohort of ACC patients RNAseq database. Nanostring PanCancer Pathway Panel was used to evaluate global genetic modifications advent from all treatment arms. A. Pathway scores from 13 pathways represented in the Nanostring PanCancer Pathway Panel were calculated using the Advanced Analysis 2.0 plugin (NanoString, USA) in a Windows operating system and R environment (The R Foundation) for each PDX tumor and treatment. Note that ACCX9 tumors present a different overall activation status of the 13 pathways represented in the Nanostring PanCancer Pathway Panel compared with ACCX5M1 and ACCX6 tumors. B. Diagram depicts two genes of interest from the Cell Cycle-Apoptosis signaling pathway from the Nanostring panel showing high expression rates on ACCX9 PDX model. C. Venn diagram depicts 3 genes commonly downregulated in the ACCX9 PDX model. D. Data from RNAseq set from 68 samples from 30 female and 38 male patients were extracted and compared with the Nanostring gene set that composes the two most discriminative pathways found in the PDX data ('Cell Cycle + Apoptosis' and 'PI3K'). Patient stratification was established using ACCX9 and ACCX5M1 expression benchmarks. E. Pie chart containing RNAseq data shows 23% of all 68 ACC patients with similar signaling pathway signature of ACCX9 and 15% with similar signature of ACCX5M1 PDX model.

models, we found that the administration of Entinostat/Cisplatin resulted in the downregulation of genes associated with the DNA damage signaling pathway. In contrast, single-agent administration of Entinostat or Cisplatin failed to downregulate DNA damage-related genes. This is particularly exciting as the DNA damage pathway was highly mutated in a whole-genome sequence study of 60 ACC tumors [9].

Perhaps one of the most exciting findings of our analyses was identifying a collection of biomarkers distributed among several pathways capable of identifying ACC patients with greater potential to respond to Entinostat/Cisplatin therapy. These findings are clinically relevant as ACCX9 tumors responded particularly well to the combination therapy presenting a TGI of 106%. This finding centers on the activation of chromatin modification, DNA damage repair, and cell cycle-apoptotic pathways in tumors responsive to therapy. All the tumor models have translocations that involve the MYB gene. ACCX9 and ACCX5M1 tumors present the classical MYB-NFIB translocation, and ACCX6 has an MYB-TGFBR3. ACCX9 also presents NOTCH1 mutations, while ACCX5M1 tumors show mutations in MAML2 that are involved in the activation of the Notch signaling. ACCX6 has a different set of mutations involved in epigenetic modifications, such as BRD2, which binds to histone H4K12, chromatin remodeling, and CREBBP, which has histone acetyltransferase activity (https://www.accrf.org). The observed mutations on epigenetic modifiers observed in ACCX6 tumors may point towards the inability of Entinostat to induce histone acetylation in any of the 5 acetylation sites found in histones H3 and H4, as we showed here.

Our findings further show that interfering with tumor histones by inducing acetylation leads to the reactivation of several TSGs. In fact, the administration of Entinostat in combination with Cisplatin results in the activation of 31 TSG. From the highly activated TSG presenting a 2-fold expression, we identified SFRP1 as being upregulated in all ACC PDX models used in our study. SFRP1, or Secreted Frizzled Related Protein 1, encodes a soluble protein that controls the Wnt signaling pathway. It binds directly to soluble Wnt proteins and Frizzled receptors [34]. We have also identified 5 additional Wnt-related TSGs upregulated in all ACC tumors, including the GSK3B, MAPK10, MAPK9, RHOA, and TP53. Similar to the activation of TSG, the administration of Entinostat/Cisplatin resulted in the downregulation of several genes, including oncogenes.

Several FGF family members have been reported mutated in ACC tumors [9], which denotes that inactivation mutations in these families are important to this tumor. ACCX6 only presents mutation in FGFRL1 and no mutations in the FGF8 gene (https://www.accrf.org). It was exciting to find our combined therapy-induced over 2-fold downregulation of FGF8 oncogene in all 3 PDX models used in this study. Other members of the FGF family, including FGF10, FGFR1, FGFR3, and FGFR4, were significantly downregulated in all 3 PDX models following the combination therapy compared to vehicle levels.

All PDX models presented a better response to the combined administration of Entinostat and Cisplatin when compared to single-agent therapy. The use of HDAC inhibitors as single agents has shown limited results in solid tumors [35]. We have previously demonstrated that HDAC inhibitors can sensitize solid tumors to chemotherapy [12, 36-38]. Estrogen-dependent breast cancer has also benefited from HDAC inhibitors. The use of Entinostat in breast cancer has led to the re-sensitization of tumors to hormonal therapy reversing tumor-resistance phenotype [39, 40]. As estrogen-dependent breast cancer responds better to HDAC sensitization therapy, we have shown that ACCX9 tumors are distinct from ACCX5M1 and ACCX6 tumors with respect to the response to Entinostat and Cisplatin combination therapy. Indeed, the administration of Entinostat and Cisplatin to ACCX5M1 tumors marginally improved TGI by 11% compared to the administration of Entinostat alone. Meanwhile, ACCX6 tumors failed to respond to single administration of Entinostat. It is difficult to assess the causes for such discrepancy in ACC response to combined therapy. One of the potential explanations is the polyclonal nature of solid tumors, which directly impacts tumor response to therapy and tumor recurrence. Our findings support the need to develop personalized therapies for ACC tumors taking into consideration their traits and the potential stratification of

tumors accordingly to their genetic makeup. With that in mind, we strive to identify potential molecular markers capable of stratifying ACC tumors with greater potential to respond to Entinostat/Cisplatin. Using the NanoString data from the ACC PDX tumors, we identified a group of 145 genes overexpressed in ACCX9 and downregulated in all other PDX models. From the list of upregulated genes, we identified 4 TSG (PPARG, WT1, MAP3K8, WNT5A) presenting a 2-fold activation in ACCX9 over ACCX5M1 and ACCX6 tumors, therefore of potential use as a molecular marker to predict improved response to Entinostat/Cisplatin. Of note, none of the identified TSG from cluster 3 are mutated in the PDX models (above 2-fold expression). PPARG (Peroxisome Proliferator-Activated Receptor Gamma) regulates gene transcription by interacting with the RXRs, or retinoid X receptors [41]. Together, the dimmer is involved in cellular differentiation, while PPARG is also reported to inhibit cellular proliferation and induce apoptosis [42, 43]. WT1 gene is found mutated in Wilms' tumor. In its wild form, WT1 is considered a TSG and a powerful transcription regulator of several receptors as the androgen [44], epidermal growth factor [45, 46], and insulin [47] receptors, among others. MAP3K8 gene is often reported as an oncogene but presents several functions related to a TSG. MAP3K8 is found within the list of TSGs used in this work [18]. MAP3K8, also known as TPL2 kinase, plays a TSG function in lung and skin carcinogenesis [48, 49], and its loss resulted in increased intestinal tumorigenesis in Apc^{min} mice [50]. The last TSG triggered by the administration of Entinostat/Cisplatin is WNT5A. In colon cancer, the presence of WNT5A represses EMT and the canonical Wnt pathway [51]. Activation of Wnt5a further disrupts tumor migration, proliferation, and invasion, all hallmarks of aggressive tumor behavior. In fact, the presence of Wnt5a impaired tumor growth in nude mice.

Cellular senescence is a biological event that is often overlooked in cancer biology. Senescent cells are unable to divide and undergo major changes in chromatin organization. Chromatin modifications result in changes in the secretion pattern of senescent cells that can drive tumor resistance to therapy [52, 53]. Using tissues from our PDX models receiving Entinostat and/or Cisplatin, we explored the cellular senescence burden in each of our models and therapies. We observed that two of our tumor models (ACCX9 and ACCX5M1) did not experience an accumulation of senescent cells upon therapy. However, we observed that ACCX6 tumors did accumulate senescent cells during the administration of Cisplatin alone or in combination with Entinostat. Interesting to note that ACCX6 tumors showed the lowest tumor growth response to Entinostat/Cisplatin administration from all PDX models used in this study while being the only tumor model with tumor growth above control levels for single-drug therapy (Entinostat, TGI = -20%; Cisplatin TGI = -29%).

Historically, science has pursued the identification of molecular markers capable of detecting incipient tumors and predicting behavior, progression, and the presence of metastasis. Molecular markers have also been used to stratify patients presenting a greater response to therapy. Such effort in identifying molecular markers has proven valuable for certain tumors like prostate cancer. The identification of high levels of PSA in the bloodstream of patients is particularly of great value in identifying early prostate cancer. Similarly, identifying p53, Bcl-2, p16INK4A, p27Kip1, and other markers has also proved to have significant prognostic value for prostate cancer [54]. Identifying markers for other common tumors also trails the advances seen in prostate cancer. Nonetheless, patients suffering from rare malignancies like ACC are less fortunate, as limited resources are available to better understand the biology of such tumors. Here we have identified a series of biomarkers capable of predicting better tumor response to the administration of Entinostat in combination with Cisplatin. However, we unveiled something unexpected using data from our targeted gene screening focusing on signaling pathways. We found that signaling pathways, rather than individual molecular markers, can predict tumor response to Entinostat/Cisplatin. Therefore, we have shown here that ACC tumors present unique genetic signatures with great prognostic value. In fact, after validation of our genetic signature in 68 ACC patients presenting RNAseq data, we found that close to a quarter of all ACC patients are likely to respond well to therapy.

Acknowledgements

The monoclonal antibody AFFN-Ki67-3EG, deposited by the EU Program Affinomics, was

obtained from the Developmental Studies Hybridoma Bank (created by the NIH Eunice Kennedy Shriver National Institute of Child Health and Human Development (NICHD) and maintained at The University of Iowa (Iowa City, IA, USA)). Thank you to Syndax Pharmaceutical for providing Entinostat for the in vivo experiments. "We acknowledge support from the Bioinformatics Core of the University of Michigan Medical School's Biomedical Research Core Facilities". Special thanks to Dr. Scott A. Ness from the University of New Mexico for kindly providing the ACC RNAseq dataset. This work was funded by the Adenoid Cystic Carcinoma Research Foundation (ACCRF) and the University of Michigan School of Dentistry faculty grant.

Disclosure of conflict of interest

None.

Address correspondence to: Dr. Rogerio M Castilho, Laboratory of Epithelial Biology, University of Michigan, 1011 N. University Ave. Room - 3150 Commons, Ann Arbor, MI 48109-1078, USA. E-mail: rcastilh@umich.edu

References

[1] Xu B, Drill E, Ho A, Ho A, Dunn L, Prieto-Granada CN, Chan T, Ganly I, Ghossein R and Katabi N. Predictors of outcome in adenoid cystic carcinoma of salivary glands: a clinicopathologic study with correlation between MYB fusion and protein expression. Am J Surg Pathol 2017; 41: 1422-1432.

[2] Ouyang DQ, Liang LZ, Zheng GS, Ke ZF, Weng DS, Yang WF, Su YX and Liao GQ. Risk factors and prognosis for salivary gland adenoid cystic carcinoma in Southern China: a 25-year retrospective study. Medicine (Baltimore) 2017; 96: e5964.

[3] Papaspyrou G, Hoch S, Rinaldo A, Rodrigo JP, Takes RP, van Herpen C, Werner JA and Ferlito A. Chemotherapy and targeted therapy in adenoid cystic carcinoma of the head and neck: a review. Head Neck 2011; 33: 905-911.

[4] Ho AS, Ochoa A, Jayakumaran G, Zehir A, Valero Mayor C, Tepe J, Makarov V, Dalin MG, He J, Bailey M, Montesion M, Ross JS, Miller VA, Chan L, Ganly I, Dogan S, Katabi N, Tsipouras P, Ha P, Agrawal N, Solit DB, Futreal PA, El Naggar AK, Reis-Filho JS, Weigelt B, Ho AL, Schultz N, Chan TA and Morris LG. Genetic hallmarks of recurrent/metastatic adenoid cystic carcinoma. J Clin Invest 2019; 129: 4276-4289.

[5] Persson M, Andren Y, Mark J, Horlings HM, Persson F and Stenman G. Recurrent fusion of MYB and NFIB transcription factor genes in carcinomas of the breast and head and neck. Proc Natl Acad Sci U S A 2009; 106: 18740-18744.

[6] Mitani Y, Li J, Rao PH, Zhao YJ, Bell D, Lippman SM, Weber RS, Caulin C and El-Naggar AK. Comprehensive analysis of the MYB-NFIB gene fusion in salivary adenoid cystic carcinoma: incidence, variability, and clinicopathologic significance. Clin Cancer Res 2010; 16: 4722-4731.

[7] Mitani Y, Liu B, Rao PH, Borra VJ, Zafereo M, Weber RS, Kies M, Lozano G, Futreal PA, Caulin C and El-Naggar AK. Novel MYBL1 gene rearrangements with recurrent MYBL1-NFIB fusions in salivary adenoid cystic carcinomas lacking t(6;9) translocations. Clin Cancer Res 2016; 22: 725-733.

[8] Stephens PJ, Davies HR, Mitani Y, Van Loo P, Shlien A, Tarpey PS, Papaemmanuil E, Cheverton A, Bignell GR, Butler AP, Gamble J, Gamble S, Hardy C, Hinton J, Jia M, Jayakumar A, Jones D, Latimer C, McLaren S, McBride DJ, Menzies A, Mudie L, Maddison M, Raine K, Nik-Zainal S, O'Meara S, Teague JW, Varela I, Wedge DC, Whitmore I, Lippman SM, McDermott U, Stratton MR, Campbell PJ, El-Naggar AK and Futreal PA. Whole exome sequencing of adenoid cystic carcinoma. J Clin Invest 2013; 123: 2965-2968.

[9] Ho AS, Kannan K, Roy DM, Morris LG, Ganly I, Katabi N, Ramaswami D, Walsh LA, Eng S, Huse JT, Zhang J, Dolgalev I, Huberman K, Heguy A, Viale A, Drobnjak M, Leversha MA, Rice CE, Singh B, Iyer NG, Leemans CR, Bloemena E, Ferris RL, Seethala RR, Gross BE, Liang Y, Sinha R, Peng L, Raphael BJ, Turcan S, Gong Y, Schultz N, Kim S, Chiosea S, Shah JP, Sander C, Lee W and Chan TA. The mutational landscape of adenoid cystic carcinoma. Nat Genet 2013; 45: 791-798.

[10] Morris LGT, Chandramohan R, West L, Zehir A, Chakravarty D, Pfister DG, Wong RJ, Lee NY, Sherman EJ, Baxi SS, Ganly I, Singh B, Shah JP, Shaha AR, Boyle JO, Patel SG, Roman BR, Barker CA, McBride SM, Chan TA, Dogan S, Hyman DM, Berger MF, Solit DB, Riaz N and Ho AL. The molecular landscape of recurrent and metastatic head and neck cancers: insights from a precision oncology sequencing platform. JAMA Oncol 2017; 3: 244-255.

[11] Li Y and Seto E. HDACs and HDAC inhibitors in cancer development and therapy. Cold Spring Harb Perspect Med 2016; 6: a026831.

[12] Almeida LO, Guimaraes DM, Martins MD, Martins MAT, Warner KA, Nor JE, Castilho RM and Squarize CH. Unlocking the chromatin of ade-

noid cystic carcinomas using HDAC inhibitors sensitize cancer stem cells to Cisplatin and induces tumor senescence. Stem Cell Res 2017; 21: 94-105.
[13] Moskaluk CA, Baras AS, Mancuso SA, Fan H, Davidson RJ, Dirks DC, Golden WL and Frierson HF Jr. Development and characterization of xenograft model systems for adenoid cystic carcinoma. Lab Invest 2011; 91: 1480-1490.
[14] Frerich CA, Brayer KJ, Painter BM, Kang H, Mitani Y, El-Naggar AK and Ness SA. Transcriptomes define distinct subgroups of salivary gland adenoid cystic carcinoma with different driver mutations and outcomes. Oncotarget 2018; 9: 7341-7358.
[15] Love MI, Huber W and Anders S. Moderated estimation of fold change and dispersion for RNA-seq data with DESeq2. Genome Biol 2014; 15: 550.
[16] Pennock ND, Jindal S, Horton W, Sun D, Narasimhan J, Carbone L, Fei SS, Searles R, Harrington CA, Burchard J, Weinmann S, Schedin P and Xia Z. RNA-seq from archival FFPE breast cancer samples: molecular pathway fidelity and novel discovery. BMC Med Genomics 2019; 12: 195.
[17] Liu Y, Sun J and Zhao M. ONGene: a literature-based database for human oncogenes. J Genet Genomics 2017; 44: 119-121.
[18] Zhao M, Sun J and Zhao Z. TSGene: a web resource for tumor suppressor genes. Nucleic Acids Res 2013; 41: D970-976.
[19] Woo XY, Giordano J, Srivastava A, Zhao ZM, Lloyd MW, de Bruijn R, Suh YS, Patidar R, Chen L, Scherer S, Bailey MH, Yang CH, Cortes-Sanchez E, Xi Y, Wang J, Wickramasinghe J, Kossenkov AV, Rebecca VW, Sun H, Mashl RJ, Davies SR, Jeon R, Frech C, Randjelovic J, Rosains J, Galimi F, Bertotti A, Lafferty A, O'Farrell AC, Modave E, Lambrechts D, Ter Brugge P, Serra V, Marangoni E, El Botty R, Kim H, Kim JI, Yang HK, Lee C, Dean DA 2nd, Davis-Dusenbery B, Evrard YA, Doroshow JH, Welm AL, Welm BE, Lewis MT, Fang B, Roth JA, Meric-Bernstam F, Herlyn M, Davies MA, Ding L, Li S, Govindan R, Isella C, Moscow JA, Trusolino L, Byrne AT, Jonkers J, Bult CJ, Medico E and Chuang JH; PDXNET Consortium; EurOPDX Consortium. Conservation of copy number profiles during engraftment and passaging of patient-derived cancer xenografts. Nat Genet 2021; 53: 86-99.
[20] Bonner WM, Redon CE, Dickey JS, Nakamura AJ, Sedelnikova OA, Solier S and Pommier Y. GammaH2AX and cancer. Nat Rev Cancer 2008; 8: 957-967.
[21] Prosser S, Orzan E and Miani C. The quantitative effects of competition on verbal intelligibility in the elderly. Acta Otorhinolaryngol Ital 1993; 13: 99-107.
[22] Kouhara H, Koga M, Kasayama S, Tanaka A, Kishimoto T and Sato B. Transforming activity of a newly cloned androgen-induced growth factor. Oncogene 1994; 9: 455-462.
[23] MacArthur CA, Shankar DB and Shackleford GM. Fgf-8, activated by proviral insertion, cooperates with the Wnt-1 transgene in murine mammary tumorigenesis. J Virol 1995; 69: 2501-2507.
[24] Bafico A, Gazit A, Pramila T, Finch PW, Yaniv A and Aaronson SA. Interaction of frizzled related protein (FRP) with Wnt ligands and the frizzled receptor suggests alternative mechanisms for FRP inhibition of Wnt signaling. J Biol Chem 1999; 274: 16180-16187.
[25] Uren A, Reichsman F, Anest V, Taylor WG, Muraiso K, Bottaro DP, Cumberledge S and Rubin JS. Secreted frizzled-related protein-1 binds directly to Wingless and is a biphasic modulator of Wnt signaling. J Biol Chem 2000; 275: 4374-4382.
[26] Ugolini F, Charafe-Jauffret E, Bardou VJ, Geneix J, Adelaide J, Labat-Moleur F, Penault-Llorca F, Longy M, Jacquemier J, Birnbaum D and Pebusque MJ. WNT pathway and mammary carcinogenesis: loss of expression of candidate tumor suppressor gene SFRP1 in most invasive carcinomas except of the medullary type. Oncogene 2001; 20: 5810-5817.
[27] Huang J, Zhang YL, Teng XM, Lin Y, Zheng DL, Yang PY and Han ZG. Down-regulation of SFRP1 as a putative tumor suppressor gene can contribute to human hepatocellular carcinoma. BMC Cancer 2007; 7: 126.
[28] Gumz ML, Zou H, Kreinest PA, Childs AC, Belmonte LS, LeGrand SN, Wu KJ, Luxon BA, Sinha M, Parker AS, Sun LZ, Ahlquist DA, Wood CG and Copland JA. Secreted frizzled-related protein 1 loss contributes to tumor phenotype of clear cell renal cell carcinoma. Clin Cancer Res 2007; 13: 4740-4749.
[29] Fukui T, Kondo M, Ito G, Maeda O, Sato N, Yoshioka H, Yokoi K, Ueda Y, Shimokata K and Sekido Y. Transcriptional silencing of secreted frizzled related protein 1 (SFRP1) by promoter hypermethylation in non-small-cell lung cancer. Oncogene 2005; 24: 6323-6327.
[30] Marushige K. Activation of chromatin by acetylation of histone side chains. Proc Natl Acad Sci U S A 1976; 73: 3937-3941.
[31] Filippakopoulos P and Knapp S. Targeting bromodomains: epigenetic readers of lysine acetylation. Nat Rev Drug Discov 2014; 13: 337-356.
[32] Persson M, Andren Y, Moskaluk CA, Frierson HF Jr, Cooke SL, Futreal PA, Kling T, Nelander S, Nordkvist A, Persson F and Stenman G. Clinically significant copy number alterations and complex rearrangements of MYB and NFIB in head and neck adenoid cystic carcinoma.

Genes Chromosomes Cancer 2012; 51: 805-817.
[33] Frierson HF Jr and Moskaluk CA. Mutation signature of adenoid cystic carcinoma: evidence for transcriptional and epigenetic reprogramming. J Clin Invest 2013; 123: 2783-2785.
[34] Veeck J, Niederacher D, An H, Klopocki E, Wiesmann F, Betz B, Galm O, Camara O, Durst M, Kristiansen G, Huszka C, Knuchel R and Dahl E. Aberrant methylation of the Wnt antagonist SFRP1 in breast cancer is associated with unfavourable prognosis. Oncogene 2006; 25: 3479-3488.
[35] Slingerland M, Guchelaar HJ and Gelderblom H. Histone deacetylase inhibitors: an overview of the clinical studies in solid tumors. Anticancer Drugs 2014; 25: 140-149.
[36] Wagner VP, Martins MD, Martins MAT, Almeida LO, Warner KA, Nor JE, Squarize CH and Castilho RM. Targeting histone deacetylase and NFkappaB signaling as a novel therapy for Mucoepidermoid Carcinomas. Sci Rep 2018; 8: 2065.
[37] Almeida LO, Abrahao AC, Rosselli-Murai LK, Giudice FS, Zagni C, Leopoldino AM, Squarize CH and Castilho RM. NFkappaB mediates cisplatin resistance through histone modifications in head and neck squamous cell carcinoma (HNSCC). FEBS Open Bio 2014; 4: 96-104.
[38] Giudice FS, Pinto DS Jr, Nor JE, Squarize CH and Castilho RM. Inhibition of histone deacetylase impacts cancer stem cells and induces epithelial-mesenchyme transition of head and neck cancer. PLoS One 2013; 8: e58672.
[39] Yeruva SLH, Zhao F, Miller KD, Tevaarwerk AJ, Wagner LI, Gray RJ, Sparano JA and Connolly RM. E2112: randomized phase iii trial of endocrine therapy plus entinostat/placebo in patients with hormone receptor-positive advanced breast cancer. NPJ Breast Cancer 2018; 4: 1.
[40] Tiedemann H. Embryonal induction and differentiation. RNA and protein metabolism in Triturus embryos. Bull Schweiz Akad Med Wiss 1966; 22: 89-96.
[41] Tachibana K, Yamasaki D, Ishimoto K and Doi T. The role of PPARs in cancer. PPAR Res 2008; 2008: 102737.
[42] Grommes C, Landreth GE and Heneka MT. Antineoplastic effects of peroxisome proliferator-activated receptor gamma agonists. Lancet Oncol 2004; 5: 419-429.
[43] Theocharis S, Margeli A, Vielh P and Kouraklis G. Peroxisome proliferator-activated receptor-gamma ligands as cell-cycle modulators. Cancer Treat Rev 2004; 30: 545-554.
[44] Zaia A, Fraizer GC, Piantanelli L and Saunders GF. Transcriptional regulation of the androgen signaling pathway by the Wilms' tumor suppressor gene WT1. Anticancer Res 2001; 21: 1-10.
[45] Menke AL, Shvarts A, Riteco N, van Ham RC, van der Eb AJ and Jochemsen AG. Wilms' tumor 1-KTS isoforms induce p53-independent apoptosis that can be partially rescued by expression of the epidermal growth factor receptor or the insulin receptor. Cancer Res 1997; 57: 1353-1363.
[46] Englert C, Hou X, Maheswaran S, Bennett P, Ngwu C, Re GG, Garvin AJ, Rosner MR and Haber DA. WT1 suppresses synthesis of the epidermal growth factor receptor and induces apoptosis. EMBO J 1995; 14: 4662-4675.
[47] Webster NJ, Kong Y, Sharma P, Haas M, Sukumar S and Seely BL. Differential effects of Wilms tumor WT1 splice variants on the insulin receptor promoter. Biochem Mol Med 1997; 62: 139-150.
[48] Gkirtzimanaki K, Gkouskou KK, Oleksiewicz U, Nikolaidis G, Vyrla D, Liontos M, Pelekanou V, Kanellis DC, Evangelou K, Stathopoulos EN, Field JK, Tsichlis PN, Gorgoulis V, Liloglou T and Eliopoulos AG. TPL2 kinase is a suppressor of lung carcinogenesis. Proc Natl Acad Sci U S A 2013; 110: E1470-1479.
[49] Decicco-Skinner KL, Jung SA, Tabib T, Gwilliam JC, Alexander H, Goodheart SE, Merchant AS, Shan M, Garber C and Wiest JS. Tpl2 knockout keratinocytes have increased biomarkers for invasion and metastasis. Carcinogenesis 2013; 34: 2789-2798.
[50] Serebrennikova OB, Tsatsanis C, Mao C, Gounaris E, Ren W, Siracusa LD, Eliopoulos AG, Khazaie K and Tsichlis PN. Tpl2 ablation promotes intestinal inflammation and tumorigenesis in Apcmin mice by inhibiting IL-10 secretion and regulatory T-cell generation. Proc Natl Acad Sci U S A 2012; 109: E1082-1091.
[51] Cheng R, Sun B, Liu Z, Zhao X, Qi L, Li Y and Gu Q. Wnt5a suppresses colon cancer by inhibiting cell proliferation and epithelial-mesenchymal transition. J Cell Physiol 2014; 229: 1908-1917.
[52] Demaria M, O'Leary MN, Chang J, Shao L, Liu S, Alimirah F, Koenig K, Le C, Mitin N, Deal AM, Alston S, Academia EC, Kilmarx S, Valdovinos A, Wang B, de Bruin A, Kennedy BK, Melov S, Zhou D, Sharpless NE, Muss H and Campisi J. Cellular senescence promotes adverse effects of chemotherapy and cancer relapse. Cancer Discov 2017; 7: 165-176.
[53] Campisi J. Aging, cellular senescence, and cancer. Annu Rev Physiol 2013; 75: 685-705.
[54] Quinn DI, Henshall SM and Sutherland RL. Molecular markers of prostate cancer outcome. Eur J Cancer 2005; 41: 858-887.

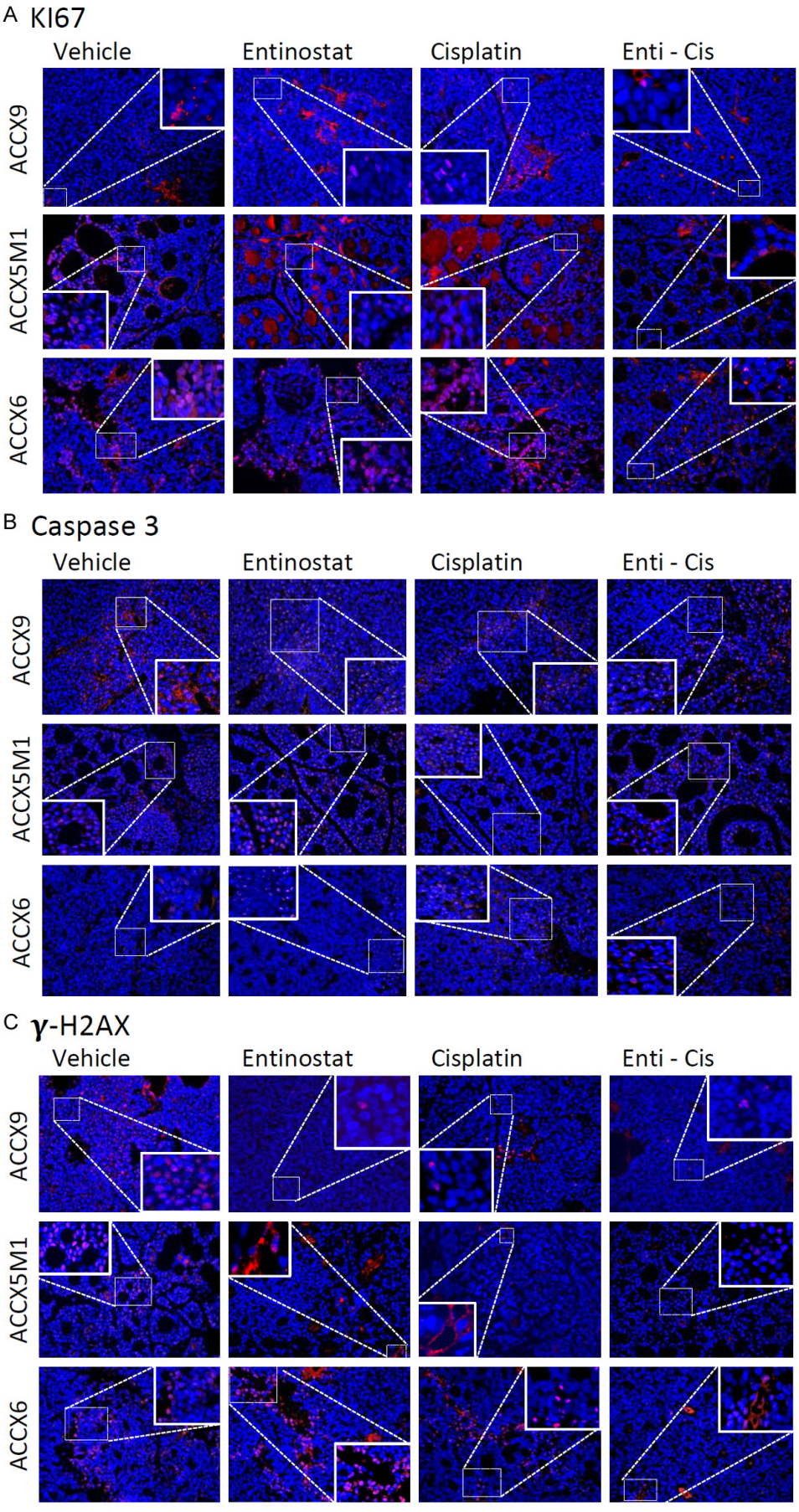
A KI67
Vehicle
Entinostat
Cisplatin
Enti - Cis
ACCX9
ACCX5M1
ACCX6
B Caspase 3
Vehicle
Entinostat
Cisplatin
Enti - Cis
ACCX9
ACCX5M1
ACCX6
C γ-H2AX
Vehicle
Entinostat
Cisplatin
Enti - Cis
ACCX9
ACCX5M1
ACCX6

Figure S1. Representative immunofluorescence images of tumor samples from ACCX6, ACCX5M1, and ACCX9 PDX models receiving Entinostat, Cisplatin, or a combination of both drugs and stained for Ki67 (A), Caspase 3 (B), and γ-H2AX (C) conjugated with Alexa 568 (red) and counterstained for DNA content using Hoechst 3342. Inserts depict the magnification of specific areas within the tumor mass.

Oncogenes identified in Cluster 1
Downregulated
(Oncogene Database)

Oncogene	ACCX9	ACCX6	ACCX5M1
CBL	↓	↓	↓
CCNE1	↓	↓	↓
CDK6	↓	↓	↓
ETS2	↓	↓	↓
EZH2	↓	↓	↓
FGF10	↓	↓	↓
FGF8	↓	↓	↓
FGFR1	↓	↓	↓
FGFR3	↓	↓	↓
FGFR4	↓	↓	↓
GLI1	↓	↓	↓
HSPA1A	↓	↓	↓
HSPB1	↓	↓	↓
JAK2	↓	↓	↓
NOTCH1	↓	↓	↓
NSD1	↓	↓	↓
PAX3	↓	↓	↓
PDGFRB	↓	↓	↓
PIK3R1	↓	↓	↓
PTCH1	↓	↓	↓
PTTG2	↓	↓	↓
SETBP1	↓	↓	↓
SPRY2	↓	↓	↓
TCL1B	↓	↓	↓
WHSC1	↓	↓	↓
WHSC1L1	↓	↓	↓

n=26 Oncogenes

↓ 2-fold downregulated over vehicle
↓ Statistical significant downregulation over vehicle

Figure S2. Table of 26 oncogenes out of the list of 130 downregulated genes identified in cluster 1 (**Figure 3A**) after administration of Entinostat + Cisplatin. Arrows in red represent 2-fold downregulation of oncogenes over vehicle, and green arrows represent statistically significant gene downregulation ($P<0.05$) in PDX tumors receiving Entinostat + Cisplatin compared with vehicle.

Tumor Suppressor Genes identified in Cluster 2
Overexpression (TSGene Database)

TSG Genes	ACCX9	ACCX6	ACCX5M1
CDH1	↑	↑	↑
CDKN1B	↑	↑	↑
CDKN1C	↑	↑	↑
CDKN2A	↑	↑	↑
CEBPA	↑	↑	↑
GAS1	↑	↑	↑
GSK3B	↑	↑	↑
HDAC1	↑	↑	↑
HDAC3	↑	↑	↑
HPGD	↑	↑	↑
ITGA7	↑	↑	↑
KLF4	↑	↑	↑
MAPK10	↑	↑	↑
MAPK9	↑	↑	↑
MSH2	↑	↑	↑
NBN	↑	↑	↑
NFKB1	↑	↑	↑
NOL7	↑	↑	↑
NUPR1	↑	↑	↑
PHF6	↑	↑	↑
PLD1	↑	↑	↑
PPP2CB	↑	↑	↑
PRKAA2	↑	↑	↑
PTPN11	↑	↑	↑
RHOA	↑	↑	↑
SFRP1	↑	↑	↑
STAT1	↑	↑	↑
TET2	↑	↑	↑
TGFBR2	↑	↑	↑
TP53	↑	↑	↑
TSLP	↑	↑	↑

N=31 TSG

↑ 2-fold upregulated over vehicle

↑ Statistical significant upregulated over vehicle

Figure S3. List of 31 tumor suppressor genes (TSG) out of a list of 127 upregulated genes identified in cluster 2 (**Figure 3A**) after administration of Entinostat + Cisplatin. Arrows in red represent 2-fold upregulation of TSG over vehicle, and green arrows represent statistical significant gene upregulation ($P<0.05$) in PDX tumors receiving Entinostat + Cisplatin compared with vehicle.

A **Cluster 3**

ACCX9 Unique Upregulated Genes (over 2-fold)

Probe Name	ACCX9	ACCX6	ACCX5M1
MYCN	5.181234	-2.79134	-1.66997
ITGA8	4.461234	-4.52134	-0.65997
SHC3	4.461234	-1.33134	-0.73997
PIK3R5	4.461234	-1.33134	-2.55997
BIRC3	3.931234	-2.52134	-2.49997
FGF14	3.931234	-2.12134	-0.85997
CALML3	3.661234	-1.33134	-1.49997
PRMT8	3.501234	-1.17134	-0.59997
MMP9	3.261234	-3.07134	-0.99997
CSF3	2.861234	-6.91134	1.590026
HOXA11	2.861234	-6.11134	-1.61997
GATA3	2.861234	-6.91134	-0.93997
SSX1	2.861234	-1.92134	-6.38997
BIRC7	2.861234	-2.12134	-1.27997
TGFB3	2.861234	-2.50134	-1.13997
PCK1	2.861234	-1.64134	-0.70997
PPARG	2.861234	-1.36134	-0.91997
WT1	2.861234	-1.03134	-1.09997
FASLG	2.691234	-3.45134	-0.96997
BAIAP3	2.661234	-1.01134	-1.06997
MAP3K8	2.651234	-1.92134	-1.01997
ZIC2	2.601234	-1.17134	-2.12997
WNT5A	2.551234	-0.94134	-0.86997
WNT2	2.431234	-0.77134	-0.96997
CAMK2B	2.371234	-2.32134	-3.70997
HMGA2	2.281234	-2.35134	-1.80997
IL1R1	2.281234	-0.91134	-0.66997
IL11	2.271234	-0.93134	-2.41997
GRIA3	2.231234	-1.25134	-0.67997
PLA2G4C	2.191234	-0.85134	-1.27997
DUSP8	2.151234	-0.91134	-0.82997
UTY	2.081234	-3.72134	-1.49997
WNT16	2.071234	-6.91134	-0.93997
IL7	2.071234	-2.92134	-2.72997
GZMB	2.071234	-4.78134	-1.84997
SOX17	2.071234	-2.12134	-1.27997
SGK2	2.071234	-2.92134	-1.14997
FGF1	2.071234	-0.85134	-0.58997
ZBTB32	2.071234	-1.01134	-1.84997
ITGB4	2.001234	-1.09134	-0.62997

B **Cluster 4**

ACCX9 unique Downregulated Genes (under 2-fold)

Probe Name	ACCX9	ACCX6	ACCX5M1
COL2A1	-6.56877	1.488662	1.670026
LAMA1	-5.46877	1.628662	1.740026
COL3A1	-4.21877	1.878662	1.830026
PDGFRA	-3.85877	1.758662	2.020026
CACNA2D2	-3.45877	1.698662	1.630026
RELN	-3.14877	1.348662	1.590026
COL1A1	-2.86877	1.348662	2.340026
TGFB1	-2.82877	1.338662	1.630026
TCF7L1	-2.80877	1.568662	2.020026
FGF7	-2.80877	2.068662	1.430026
CREB3L1	-2.37877	1.318662	2.380026
COL11A1	-2.36877	1.428662	1.830026
PDGFB	-2.35877	1.838662	1.760026
ARNT2	-2.22877	1.538662	1.610026
COL5A1	-2.19877	1.308662	1.980026
FZD2	-2.07877	1.408662	1.720026

Figure S4. A. List of genes derived from cluster 3 (**Figure 3D**) presenting a 2-fold increase in gene expression on ACCX9 PDX compared with ACCX6 and ACCX5M1 upon receiving Entinostat + Cisplatin combination therapy. B. List of genes from cluster 4 (**Figure 3D**) presenting downregulation of gene expression on ACCX9 PDX compared with ACCX6 and ACCX5M1 upon receiving Entinostat + Cisplatin combination therapy.

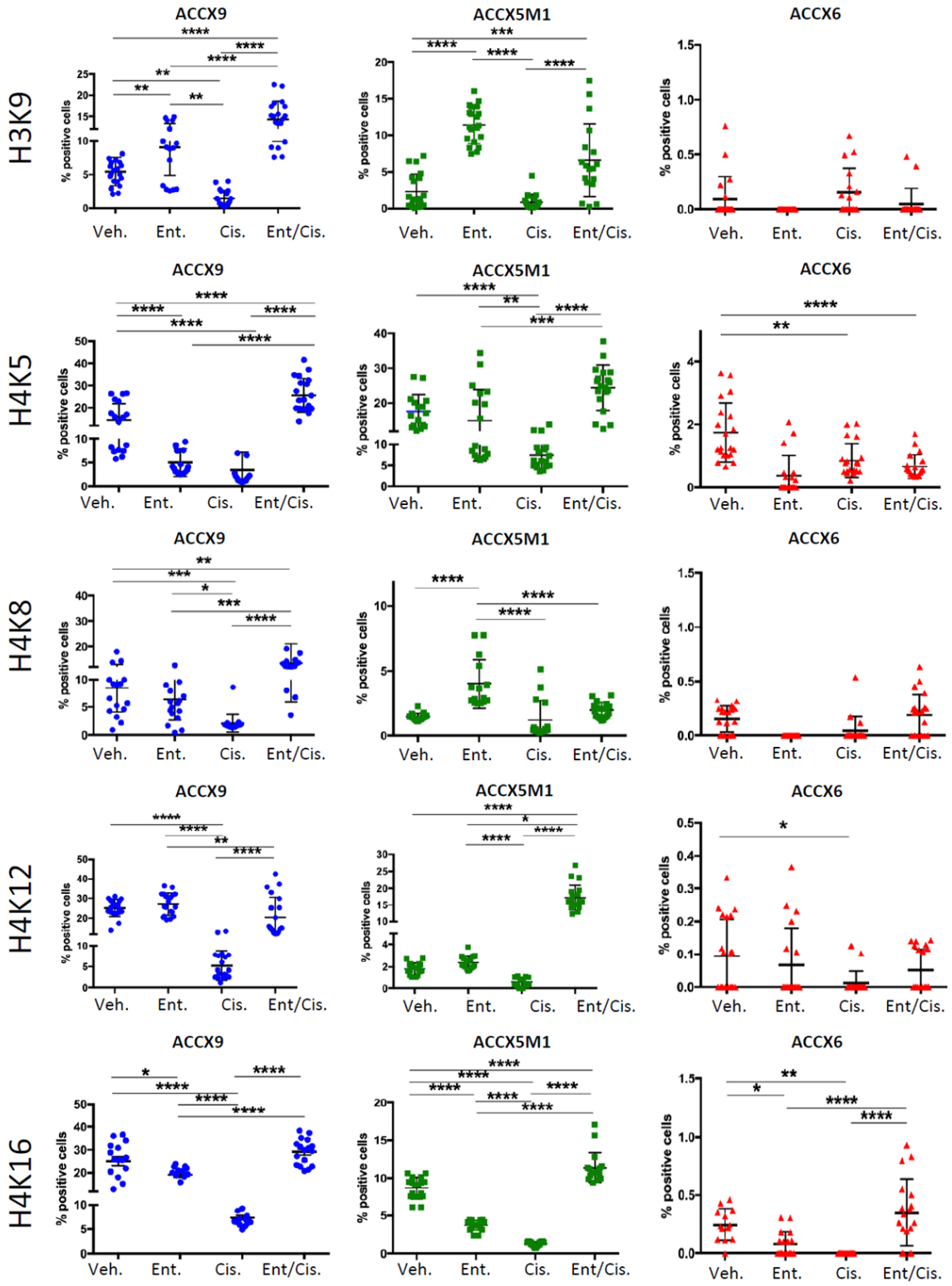

Figure S5. Tumor-specific histone acetylation levels of histones H3 lysine 9, H4 lysine 5, H4 lysine 8, H4 lysine 12, and H4 lysine 16 distributed by treatment arms (*P<0.05; **P<0.01; ***P<0.001; ****P<0.0001).

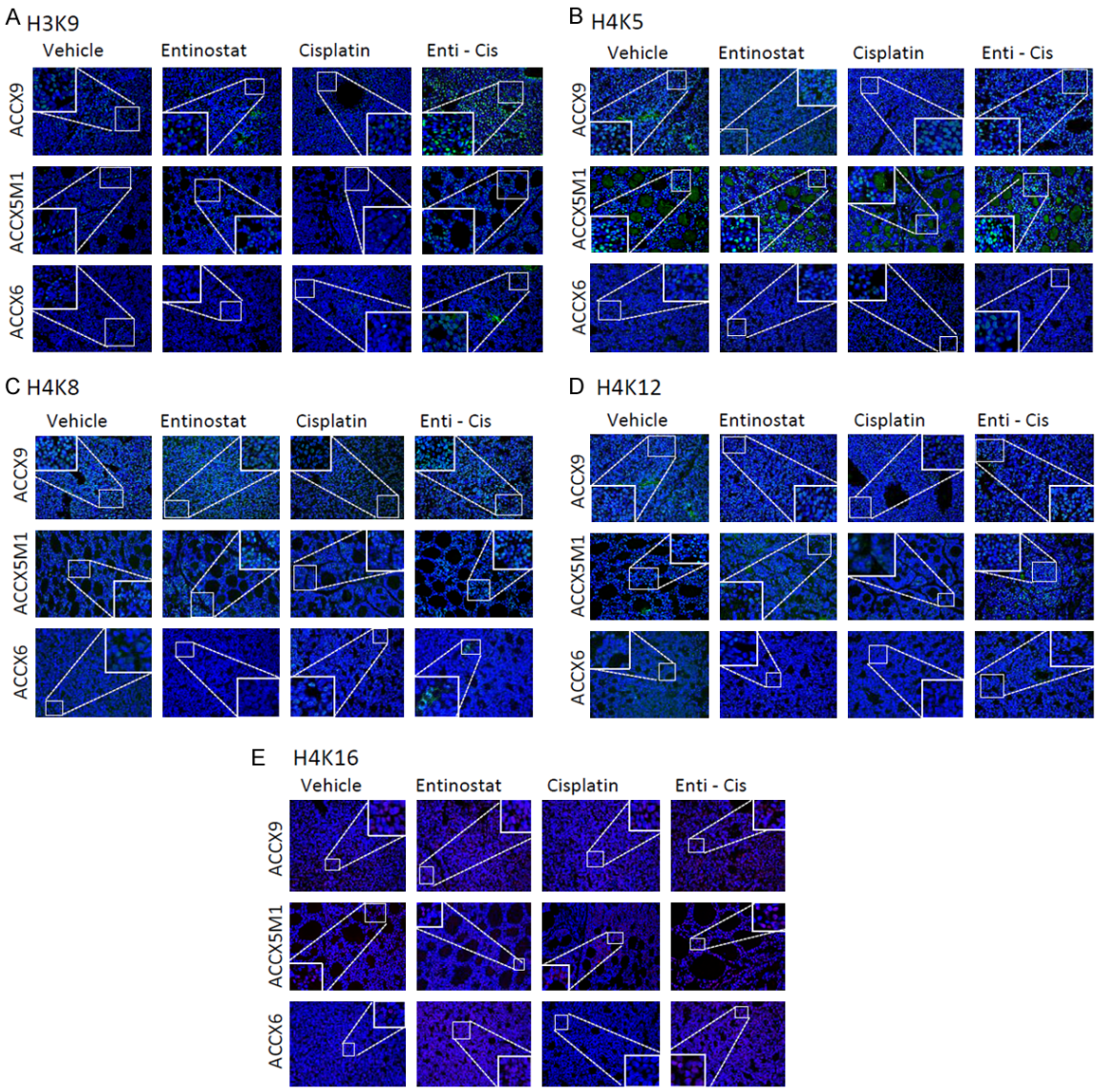

Figure S6. Immunofluorescence images of the PDX tumors ACCX6, ACCX5M1, and ACCX9 receiving Entinostat, Cisplatin, or the combination of both drugs stained for histone H3 and H4 acetylation at specific lysines (Alexa 488_green). DNA content is identified by Hoechst 3342 staining, and inserts depict the magnification of specific areas within the tumor mass.

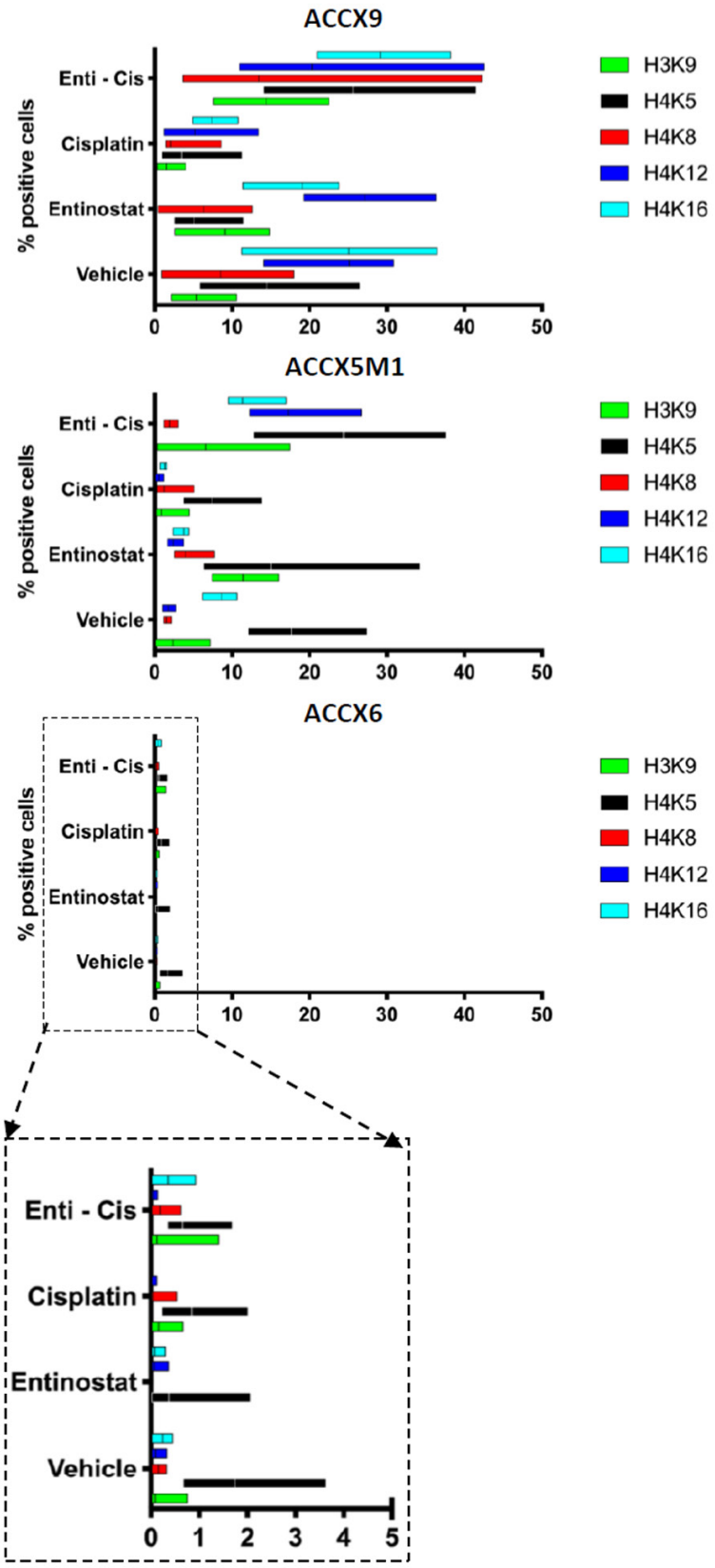

Figure S7. Bar graphic depicting the percentage of positive cells distributed by each therapeutic arm for all 3 PDX models of ACC tumors and stained for H3 lysine 9, H4 lysine 5, H4 lysine 8, H4 lysine 12, and H4 lysine 16. Note that all therapy arms failed to induce robust histone acetylation on ACCX6 compared with ACCX9 and ACCX5M1.